THE ASTRONOMICAL JOURNAL VOLUME 109, NUMBER 1 JANUARY 1995

CATALOGUE OF GALACTIC GLOBULAR-CLUSTER SURFACE-BRIGHTNESS PROFILES

S. C. TRAGER
UCO/Lick Observatory and Board of Astronomy and Astrophysics, University of California, Santa Cruz, California 95064
Electronic mail: sctrager@lick.ucsc.edu

IVAN R. KING[1]
Department of Astronomy, University of California, Berkeley, California 94720
Electronic mail: king@glob.berkeley.edu

S. DJORGOVSKI[1,2]
Palomar Observatory, California Institute of Technology, Pasadena, California 91125
Electronic mail: george@deimos.caltech.edu

Received 1994 August 4

ABSTRACT

We present a catalogue of surface-brightness profiles (SBPs) of 125 Galactic globular clusters, the largest such collection ever gathered. The SBPs are constructed from generally inhomogeneous data, but are based heavily on the Berkeley Globular Cluster Survey of Djorgovski & King. All but four of the SBPs have photometric zero points. We derive central surface brightnesses, King-model concentrations, core radii, half-light, and other fraction-of-light radii where data permit, and we briefly discuss their use.

1. INTRODUCTION

There has long been a need for a complete sample of surface-brightness profiles (SBPs) of the Galactic globular clusters for use in dynamical and evolutionary studies. Unfortunately, SBPs extending from near the cluster center to the tidal radius exist for only a limited number of clusters [see King (1966b) and Illingworth & Illingworth (1976) for a few examples], and most studies have determined dynamical parameters from separate fittings of models to the core and tidal-limit regions (cf. Peterson & King 1975). Some recent studies, such as those of Grabhorn *et al.* (1992) and Fischer *et al.* (1993) have overcome these difficulties, either by a piecemeal method similar to the one used here (in the case of Grabhorn *et al.*) or by wide-field CCD imaging and mosaicing (by Fischer *et al.*), but these studies are limited to a few clusters. We provide here SBPs for 125 Galactic globular clusters, including many clusters without previously published SBPs, of which 121 have photometric zero points. We also present central surface brightness (for those clusters with photometric zero points), fraction-to-light radii, core radii, and King (1966a) concentrations for these clusters. These data should provide a wealth of information for dynamical and evolutionary studies.

The SBPs are primarily drawn from a comprehensive photometric survey of Galactic globular clusters by Djorgovski & King (1984, 1986), who searched for evidence of core collapse. CCD SBPs of the cluster centers make up the bulk of the data, supplemented by a variety of other techniques, including digitized photographic and photoelectric photometry in the inner regions of some clusters and photographic star counts in the outer regions of many clusters.

We describe the observations and datasets used in Sec. 2. The construction of the SBPs is discussed in Sec. 3. The SBPs themselves and derived structural parameters are presented in Sec. 4. We finish with a summary and future prospects in Sec. 5.

2. DATASETS

Until the advent of large-format CCDs and mosaicing techniques in the late 1980s, no single observational technique could homogeneously cover the entire SBPs of even a moderate-sized globular cluster. We have thus combined our own CCD and photographic observations with several other observational methods to generate our SBPs.

2.1 The Berkeley Globular Cluster Survey

The Berkeley Globular Cluster Survey (Djorgovski & King 1984, 1986; Djorgovski & Penner 1985; Djorgovski *et al.* 1986) observed over 115 clusters from both the Lick Observatory and the Cerro Tololo Inter-American Observatory (CTIO) in the early to mid-1980s. A vast majority of this sample, 108 clusters, was imaged with small-format CCDs at one of the observatories (or in a few cases, at both). Short direct exposures were taken with the shortest-wavelength filters available and practical. At Lick Observatory, a TI 500^2 chip and a GEC 575×385 chip were used on the Nickel 1 m reflector, but the Spinrad red filter was the only filter available (cf. Djorgovski 1985). At CTIO, a GEC 575×385 chip with B, V, and R filters was used, as was an RCA 512×320 with U, B, V, R, and I filters, both chips on the 1.5 m reflector. The seeing was generally 2–3 arcsec. Djorgovski & King (1986) provide a more complete description. Some additional clusters were imaged, but difficulties with interstellar absorption or data transfer and storage made reductions of

[1]Visiting Astronomer, Cerro Tololo Inter-American Observatory. CTIO is operated by AURA, Inc. under contract to the National Science Foundation.
[2]Presidential Young Investigator.

the frames unfeasible. In one case, Terzan 5, our images were unsuitable, and Dr. T. Armandroff kindly provided an I-band image taken at CTIO, which we reduced in an identical fashion to our own CCD images. A few clusters were observed in the ultraviolet with plates taken at CTIO and digitized on the Berkeley PDS-microdensitometer; see Djorgovski & King (1984) for a complete description.

The observations, both photographic and CCD, were reduced using the method outlined by Djorgovski (1988). A brief outline of the process follows. Foreground stars are removed by eye examination of each image; the procedure is to mark each star that is obviously too bright to be a cluster member and to remove an area around it from the data. (Since all surface brightnesses are derived as counts per unit area, any area can be arbitrarily removed.) Next, a cluster center is found using the "mirror-autocorrelation" technique developed by I.R.K. Poor centering is still a problem, especially in loose, ragged clusters, manifesting itself as an unphysical depression in the central regions of the SBP. A SBP is derived by dividing the image into concentric apertures which are then subdivided into octants. The mean brightness and standard deviation of the octants of a given aperture are measured to determine internal errors due to the noisy nature of light profiles of globulars. Finally, a sky brightness is determined from clear regions of the corners of the images and subtracted from the SBP. This can introduce errors in the outermost apertures of the SBP, but these are easily noticed and given low weights in our profile-building routine described in Sec. 3.

2.2 *"Secondary" Datasets*

In a number of well-studied clusters, photoelectric surface-brightness measurements either supplement our SBPs or, in some cases, stand in the stead of our CCD data. Photoelectric surface-brightness measurements from Gascoigne & Burr (1956), King (1966b), Illingworth & Illingworth (1976) [which includes data taken from the studies of Kron & Mayall (1960) and of Kron (1966)], and Da Costa (1979) provide not only very accurate data in the central regions of clusters but also photometric zero points (see Sec. *3.2.2*). Both centered-aperture and scan measurements, if present, are used, though centered-aperture measurements are more accurate. Scan measurements are useful to connect star counts to the central parts of the SBP. Twenty clusters in our sample have photoelectric surface-photometry measurements.

In the outer envelopes and tidal-limit regions of clusters, our primary data consist of photographic star counts from Kinman & Rosino (1962), King *et al.* (1968), Illingworth & Illingworth (1976), Peterson (1976), and DaCosta (1982). In these studies, a réseau, typically divided into 36 radial sectors and 30 concentric apertures, is placed over photographic images, and stars are counted in each sector with a binocular microscope or a microfilm projector. Occasionally a square réseau is used instead but the counts are transformed into annular measurements. Photographic star counts have two deficiencies that limit their usefulness, however. First, towards the interior of the cluster, crowding of the stars makes determination of the number density difficult. King *et al.* (1968) make an empirical correction for this effect, but points corrected in this manner are of decreased reliability. However, the corrected points are better (in most cases) than the uncorrected points, which underestimate the true surface brightness as estimated from the rest of the SBP. Second, the faintest star counts (primarily those made from Polamar 5 m plates) sample stars of lower mass than those that contribute the majority of the light in the other datasets, which are primarily giants, horizontal-branch, and turnoff stars. Since these low-mass stars are expected to have a different distribution, they have been excluded. Finally, it should be noted here that star counts from plates taken at the Boyden Observatory [noted SB, ADH, and A in our SBPs; see King *et al.* (1968)] were discovered in the course of this work to be often quite discrepant from other measurements (see Secs. 3 and 4).

Finally, in the case of IC 4499, we differentiated concentric-aperture photoelectric photometry from Peterson's (1987) catalogue to derive a SBP following the algorithm of King (1988). This procedure will be discussed at length in Sec. 3, as it was used to determine photometric zero points of a number of clusters.

2.3 *"Tertiary" Datasets*

These datasets serve some purpose subsidiary to the primary and secondary data, such as connecting the star counts to the photometry in the central regions, but for profile tracing they are less reliable than the other datasets. Electronographic photometry belongs to the former category; the crowding-corrected star counts fall into the latter category.

Electronographic photometry of Kron *et al.* (1984) serves to connect the inner CCD, photoelectric, or photographic photometry to the outer photographic star counts in many clusters. However, these data are hampered during reduction by intentional defocusing and possible centering errors. These problems combine to degrade data within 5 or 6 arcsec of the cluster center. Inaccuracies in the determination of sky background levels also weakens agreement with the SBPs in the outer envelopes of the clusters. In spite of these problems, reasonable agreement of the electronographic photometry from the edge of the core to the envelope is typical, providing a useful bridge from central photometry to star counts. These data form a large subsample of the data presented, with 69 of 125 clusters having electronographic photometry from this catalog.

Additionally, electronographic photometry of M15 (NGC 7078) was taken from the study of Newell & O'Neil (1978). These data do not suffer the same defocusing at the cluster core as do the data of Kron *et al.* (1984), as these data were taken in an attempt to probe the core M15 for signs of dynamical collapse and consequent deviation from a King profile.

Several additional datasets are used, notably microdensitometer traces of photographic plates taken for Peterson & King (1975). Star counts by Bahcall and collaborators (Bahcall 1976; Bahcall *et al.* 1977) were examined but were found difficult to reconcile with the profiles and were not used.

3. SBP CONSTRUCTION

We outline the construction of SBPs from the datasets discussed in Sec. 2. The process consists of three stages: a preliminary hand fitting of the best of the primary data and of the secondary data, to produce a smooth curve; a determination of the zero-point shift of each primary dataset to the profile; and finally, an iterative polynomial-fitting/dataset-shifting routine to produce the final, smooth profile with a zero-pointed surface-brightness scale.

A cautionary note: In combining of datasets, we have implicitly assumed that color does not vary with radius, or have explicitly avoided this complication, as was done in the determination of the $B-V$ correction for the photoelectric-photometry zero points (Sec. *3.2.2*). This allows matching of star counts taken in B with CCD photometry in R, for example; but ignoring the color gradients runs the risk of deformed profiles if the gradients are significant. Such effects are negligible for most of our clusters, as color gradients have not been observed in any King-model clusters to date (cf. Djorgovski & Piotto 1993), which are in a majority in this study.

3.1 Initial SBP Construction

As a first pass for most of the clusters, the SBP determined from the shortest-wavelength, longest-exposure (but not saturated) CCD frame was plotted as log of intensity (with an arbitrary zero point) against log of radius. Electronographic photometry and photographic star counts were then introduced and shifted arbitrarily in log intensity until the profiles looked smooth by eye.

3.2 Determination of Photometric Zero Points

Photometric zero points for the SBPs were derived by one of four methods, which we list in order of frequency of use: (1) if CCD or photographic photometry existed, without photoelectric surface brightnesses, then a growth-curve fitting process was used; (2) if detailed photoelectric surface-brightness photometry existed, a zero point was taken directly from this photometry; (3) if star counts were the only dataset available for the profile, Peterson's (1987) catalogue was used to directly compute a surface brightness at some given radius (or, in the case of IC 4449, at several radii); or, failing any of the preceding, (4) the total light contained within the profile was compared with a total magnitude taken from Peterson (1993). In four cases (Ton 2, Terzan 7, Terzan 11, and Palomar 10), no photometric zero point was available by any of these methods.

3.2.1 Growth-curve fitting

In clusters with CCD or photographic photometry but no photoelectric surface-brightness measurements, a growth curve was constructed from a table of total counts converted to an arbitrary magnitude scale as a function of radius. This growth curve was then plotted against a V-band growth curve taken from Peterson's (1987) compilation of concentric-aperture magnitudes. The magnitude difference of the two growth curves then gave the photometric zero point of the SBP. Figure 1(a) shows a good fit of a CCD growth curve to a Peterson growth curve; Figure 1(b) shows a poor fit. It should be noted that photoelectric photometry from Rousseau (1964) and Hanes & Brodie (1985) are omitted in the construction of growth curves from Peterson's catalogue, as they were too frequently found to be discrepant with the other data in this catalogue.

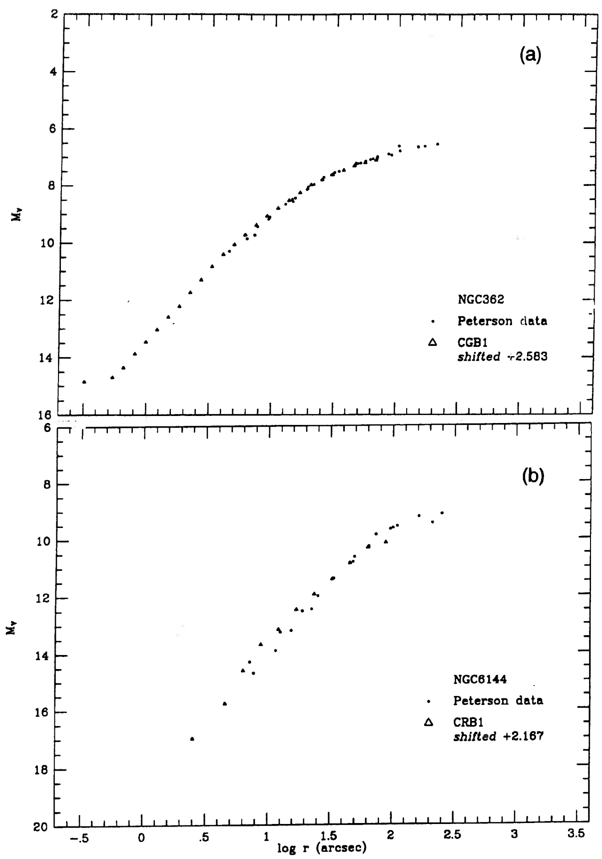

FIG. 1. Examples of growth-curve fitting to derive photometric zero points. Solid dots are photoelectric concentric-aperture photometry data from Peterson (1987); open triangles are CCD data. (a) A good fit of CCD data to photoelectric photometry. The CCD data were taken with the GEC chip at CTIO with a B filter. (b) A poor fit of CCD data to photoelectric photometry. The CCD data were taken with the RCA chip at CTIO with a B filter.

3.2.2 Photoelectric surface-brightness zero points

For the 20 clusters with photoelectric surface-brightness measurements, a photometric zero point was determined directly from the photoelectric measurements. However, zero points for ten of these clusters are in the B band, so mean $B-V$ values needed to be determined. This correction was found by plotting $B-V$ against radius from Peterson's catalogue and averaging over a suitable range of radius. To avoid color-gradient effects a minimum radius, interior to which points were excluded from the average, was chosen by inspection of the plots of $B-V$ against radius. This average $B-V$ value is noted on the SBP plots of the relevant clusters. In the case of NGC 6397, the color gradient noted by Djorgovski & Piotto (1993) and others was explicitly avoided merely by shifting DaCosta's (1979) B photometry onto Peterson's (1987) data and determining $B-V$ by eye.

3.2.3 *Other zero points*

For a few clusters where the SBP had to be constructed solely from star-count data, and concentric-aperture photoelectric photometry measurements were available, a surface brightness at some radius was constructed from Peterson's (1987) catalogue following the prescription of King (1988): Given two photometric points with radii r_1 and r_2 and corresponding magnitudes m_1 and m_2, the surface brightness at some intermediate point r_e is

$$\mu=-2.5\ \log\left[\frac{10^{-0.4m_2}-10^{-0.4m_1}}{\pi(r_2^2-r_1^2)}\right].$$

If both r_1 and r_2 are greater than the core radius r_c, then

$$r_e=\sqrt{\frac{r_2^2-r_1^2}{2\ \ln r_2/r_1}};$$

otherwise

$$r_e=\sqrt{\frac{r_2^2-r_1^2}{\ln(r_c^2+r_2^2)/(r_c^2+r_1^2)}-r_c^2}.$$

These formulas were also used to construct a SBP from Peterson's catalogue data for IC 4499, as mentioned in Sec. 2.

The clusters AM 1, Palomar 1, and Palomar 4 have no surface-brightness measurements in Peterson's catalogue; for these clusters, the total light contained within the profile (suitably extended by an exponential cutoff, if necessary; see the discussion of fraction-of-light radii in Sec. 4) was compared with a total V magnitude from the tabulation of Peterson (1993), and a photometric zero point was derived directly from this difference.

3.3 *Final SBP Construction*

Finally, Chebyshev polynomials were fit to the zero-pointed SBPs. (See below for the choice of the Chebyshev form.) These polynomial fits were used as templates against which to refine the offsets of the nonzero-pointed datasets (basically, every dataset except photoelectric, photographic, and CCD photometry) and to shift all previously unused datasets to the SBP. These polynomials also have the advantage of providing "quick-look" versions of the SBPs, though they should not be used for detailed theoretical or observational studies.

In order to keep the polynomials physically realistic near the core, a "core-correction" mechanism was developed. King (1962) showed that a function of the form

$$\frac{f}{f_0}=\frac{1}{[1+(r/r_c)^2]},$$

where f is the surface brightness at radius r, f_0 is the central surface brightness, and r_c is the core radius, empirically describes SBPs of normal (i.e., non-post-core-collapse) clusters from the center to the midenvelope (though not out to the tidal radius, as this function has no tidal turn-down). For each cluster in the sample, a rough core radius was determined by fitting a multimass King (1966a) model of moderate concentration to the core region of the cluster. For the normal clusters, the SBP was transformed by

$$\log x=\log[1+(r/r_c)^2],$$

where x is a new dimensionless radius; however, the post-core-collapse clusters (as noted by Djorgovski & King 1986) were not transformed in this manner. This core correction flattens out the core regions in a satisfactory way, and its effect does not seem to be strongly dependent on the exact value of r_c chosen.

To allow for the differing quality of our inhomogeneous datasets, each dataset was given a global weight and each data point an individual weight. A dataset was assigned a weight on the basis of its overall quality, with our CCD and photographic photometry and the "secondary" datasets receiving higher weights than the tertiary datasets (see the discussion in Sec. 2). Individual data in each set were then assigned weights that depended on their relative internal errors. This "by-eye" weighting procedure was used in place of rigorous relative errors for two reasons: (1) only close approximations of the profiles are needed for the polynomial fits, whose primary purpose is to put all the datasets onto a common surface-brightness scale; and (2) several datasets do not have well-determined errors. For example, crowding-corrected star-count data and data of the electronographic photometry near the innermost and outermost radii are given low weight, as are the outermost data of some CCD photometry in which the sky value is judged to be questionable. Additionally, electronographic photometry and photographic star counts from the Boyden Observatory [SB, ADH, and A plates, which tend to be discordant with other datasets; see King 1966(a)] are given low global weights.

The data and their weights were fed into a least-squares polynomial fitting routine (taken from Press *et al.* 1989), using Chebyshev polynomials as the fitting functions. Since Chebyshev polynomials are useful only in the interval $[-1,1]$, the data, which may have been core corrected by the algorithm above, were transformed onto this interval, using the innermost and outermost radii that had not been weighted zero. The weighted mean residual of each dataset was used to shift the dataset in the log-surface-brightness coordinate to (usually) a single CCD or photographic-photometry dataset or that of any photoelectric photometry (which includes the SBP constructed for IC 4449, as discussed in Sec. *3.2.3*). This process was repeated, fitting and shifting, until the weighted mean residuals of each dataset in the SBP changed by less than $\Delta\mu_V=0.005$. False convergences were occasionally reached, but these were easy to recognize and correct by small changes in the initial offsets.

At each iteration in the polynomial fitting process, the Chebyshev polynomial was truncated, if possible, at the lowest order for which all polynomials of higher order had coefficients less than μ_V=0.100. (The ability to economize in this way was our main reason for choosing Chebyshev polynomials. But also, Chebyshev polynomials of low order are very close to having the smallest possible maximum deviation from the true function being approximated, among all polynomials of that order. When the high-order coefficients of a Chebyshev polynomial are small, the lower-order truncation still provides an excellent approximation to the true SBP.) We chose a rather loose truncation criterion here, because tighter criteria produce the unphysical bumps and wiggles that tend to appear in high-order polynomials. This truncation mechanism can be bypassed, if a polynomial fit of a given order is desired, which is occasionally necessary.

4. SBPs AND DERIVED STRUCTURAL PARAMETERS

4.1 The Profiles and Their Quality

In Fig. 2, we plot the SBPs of the 125 clusters for which we have gathered data. Solid points represent the primary and most of the secondary data; hollow points represent crowding-corrected star-count data and should be treated with some suspicion (Sec. *2.2*); and crosses represent electronographic photometry data.

In general, the polynomials provide good fits to the data or at least give a reasonable qualitative feel as to the shape of the profile. The final Chebyshev-polynomial curve is plotted against each profile as a dashed line. The typical order of the Chebyshev polynomials used for fitting ranges between second and fifth, though four profiles (NGC 4372, a sparsely studied cluster, NGC 6528, NGC 6642, and Ton 2) are fit reasonably well with a first-order Chebyshev polynomial (i.e., a straight line), and two profiles (NGC 6544, and Palomar 12, although the data for this cluster are somewhat suspect—the CCD photometry data form a very rough, bumpy profile with little physicality) are fit with a sixth-order Chebyshev polynomial. For one cluster, NGC 6101, a second-order fit is forced upon the cluster with some success after problems with higher-order polynomials, such as unphysical bends. The polynomials do not show, however, the tidal turn-down for most clusters [though a few clusters, such as NGC 104 (47 Tuc) are well observed into the turn-down]; to have the polynomials follow the tidal turn-down would require a foreknowledge of the tidal radius, which is not possible for many clusters. Though the core correction does not depend strongly on the exact value chosen for the core radius (as discussed briefly in Sec. *3.3*), forcing a tidal turn-off seems unwise for most clusters. Where two primary datasets disagree, the polynomials, as expected, follow the middle path; this is occasionally a problem, such as in the profiles of NGC 4147 (where the shape of the profile makes fitting near the core difficult) and NGC 6093 (where the slopes of the photographic and photoelectric photometry data do not follow that of the CCD photometry). It should be noted that the poorest curves generally belong to ragged clusters of low surface brightness.

It was mentioned in Secs. 2 and 3 that photographic star counts from Boyden Observatory plates are somewhat less reliable than other star counts. On examination of the profiles, we noticed that nearly all star-count data from plates taken at the Boyden Observatory (these include SB, ADH, and A plates) seem in discord with other star-count data (e.g., see the profile of NGC 362, and notice the disagreement of the star counts from the ADH plate with the counts from the UP plate). Data from these plates typically do not affect the shape of the profiles because of the low weights given to individual data points, but photographic star-count data from these plates are given less global weight in the fitting procedure. Discrepancies in counts from the SB and A plates are understandable, because the former often gave bad images and the latter had off-axis aberrations; but it is a mystery why counts from the ADH Baker–schmidt should be discrepant.

The profile data (along with polynomial coefficients) will be published in the ApJ/AJ CD-ROM Series. Table 1 shows a sample of this file, for one cluster (NGC 6584).

4.2 Structural Parameters

With a final profile in hand, we can determine a number of useful parameters: concentration c, core radius r_c, central surface brightness $\mu_V(0)$, a half-light radius r_h, and other fraction-of-light radii. We summarize the procedure here; a detailed discussion appears in Trager *et al.* (1993).

A grid of single-mass, nonrotating, isotropic King (1966a) models is fitted to the profile, and a value of the concentration parameter c is read off. The Chebyshev polynomial gives the value of the central surface brightness $\mu_V(0)$: the innermost point of the fit gives $\mu_V(0)$, unless the fit is somehow unstable (as is the case in some post-core-collapse clusters), in which case the brightest value of μ_V is taken. The central surface brightness then gives the HWHM of the SBP, which is used to derive r_c using c by interpolating in the table of Peterson & King (1975). For most apparently post-core-collapse clusters, we set r_c=HWHM and c=2.5 if no better fit can be obtained. All of our core radii measurements less than 2 arcsec should be regarded as upper limits, due to the seeing blur of the images used.

We compared these measurements with those of Chernoff & Djorgovski (1989), who used nearly the same observational material, but a different methodology. The agreement is generally excellent, but in a few discrepant cases (typically ragged, poor clusters) we adopted the values of Chernoff and Djorgovski.

We evaluated the half-light, r_h, and fraction-of-light radii (from $r_{10\%}$ to $r_{40\%}$) for each cluster with a polynomial-fitting procedure developed originally by Dr. J. J. González. The reliability of the resultant radii depends on the radial coverage of the profile, with SBPs covering larger fractions of the total light being more reliable.

We compared our r_h measurements with those of van den Bergh *et al.* (1991), who used Peterson's (1987) compilation and a different methodology. The agreement is generally quite good. Assuming that both sets of measurements contribute equally to the scatter, we estimate that our typical 1σ

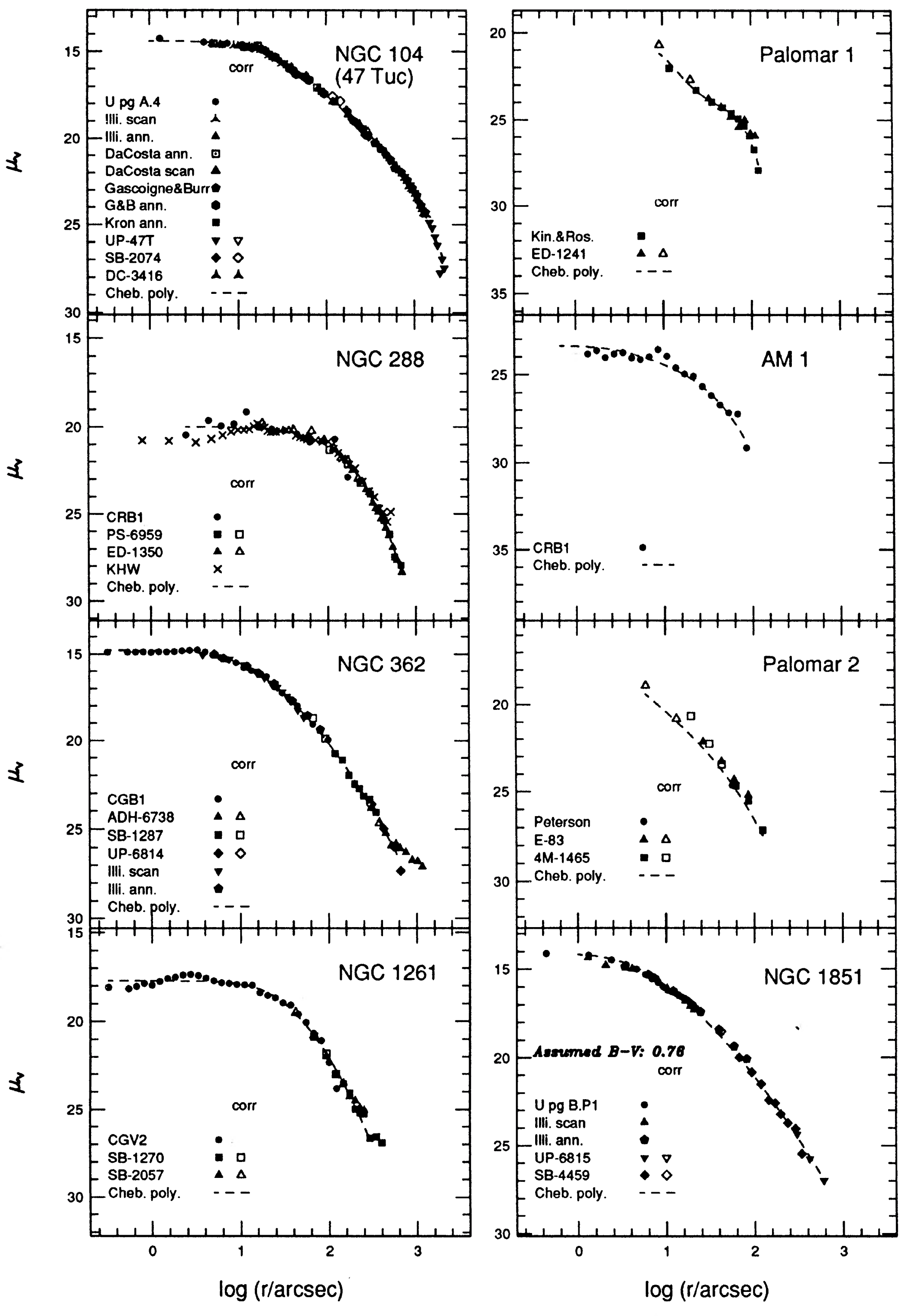

FIG. 2. The SBPs. The CCD data follow a naming convention: "*C*" stands for data taken at CTIO; e.g., "CRB1" stands for the first "*B*" image from the CTIO 1.5 m reflector with the RCA chip. "*L*" stands for the Lick 1 m Nickel reflector: these datasets are labeled as, e.g., "LTR-B," the second frame from the Lick Nickel reflector, taken with the TI chip through the Spinrad "*R*" filter. See Sec. *2.1* for details of chips and filters. "DJB2" stands for the second "*B*" image taken by Djorgovski. For Terzan 5, "*I*" refers to an *I*-band image from CTIO kindly provided to us by Dr. T. Armandroff. "U pg A.4" means the first ("A") ultraviolet ("U") plate used for photographic photometry ("pg") of the cluster in question. "Scan" data are scanning photoelectric photometry. "Ann" data are centered-aperture photoelectric photometry. Photographic star counts are referenced by plate number; see King *et al.* (1986), Peterson [(1976), labeled "C-" and "CF-," as well as a few without alphabetic prefix], and DaCosta [(1982), labeled "DC-"]. "Kin & Ros" are star counts from Kinman & Rosino (1962) (continued on p. xxxx).

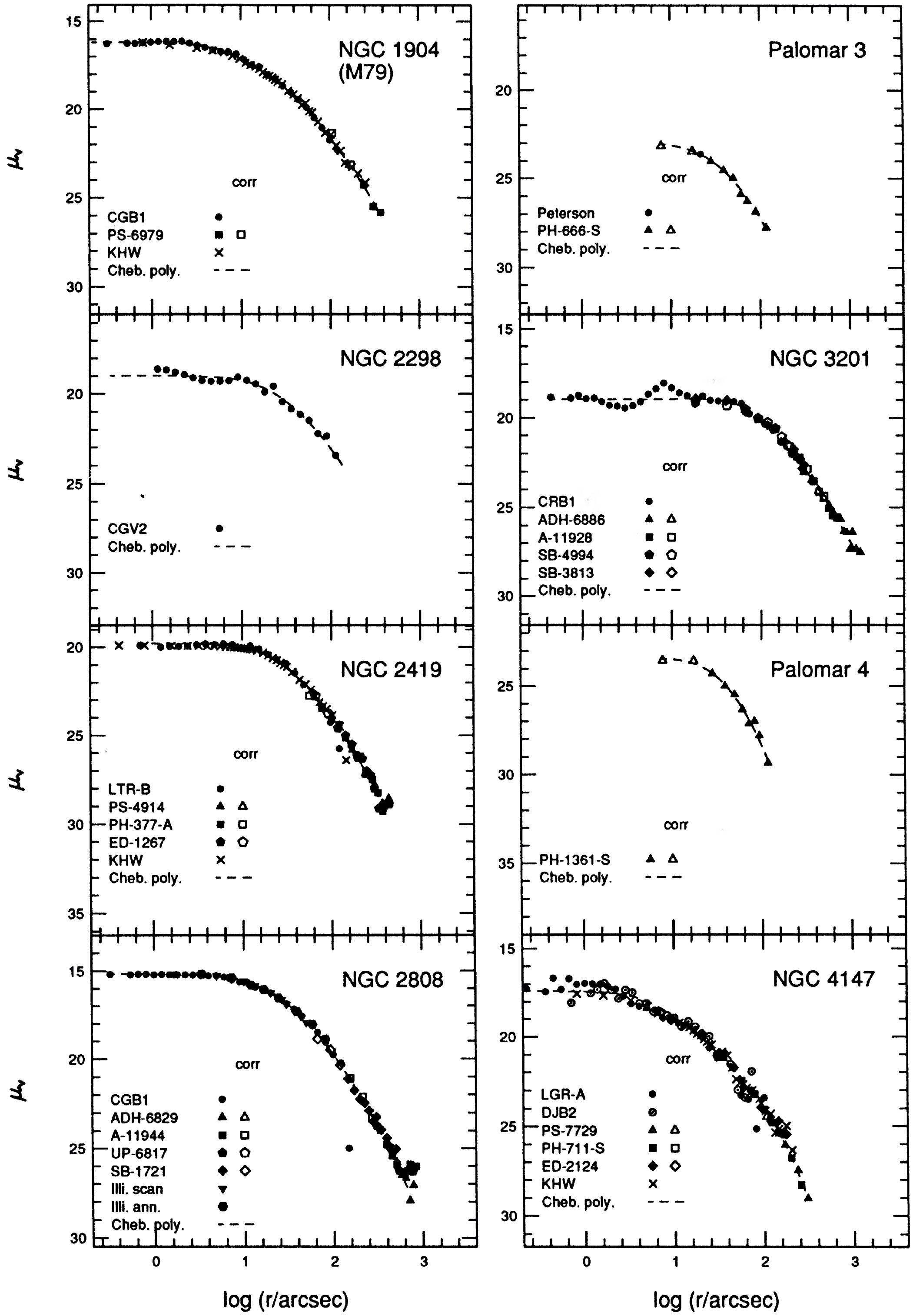

FIG. 2. (continued)

"Illi" data are from Illingworth & Illingworth (1976); "Gascoigne & Burr" and "G & B" from Gascoigne & Burr (1956); "Kron" from Kron (1966); "King" from King (1966b); "New & O'N" from Newell & O'Neill (1978); "DaCosta" and "DC" from DaCosta (1979); and "KWH" from Kron *et al.* (1984); "PK" are microdensitometer traces from Peterson & King (1975). Data labeled "Peterson" are surface-brightness points derived from Peterson (1987); see Sec. *3.2.3*. Dashed lines are Chebyshev polynomials fit to the profiles (labeled "Cheb poly").

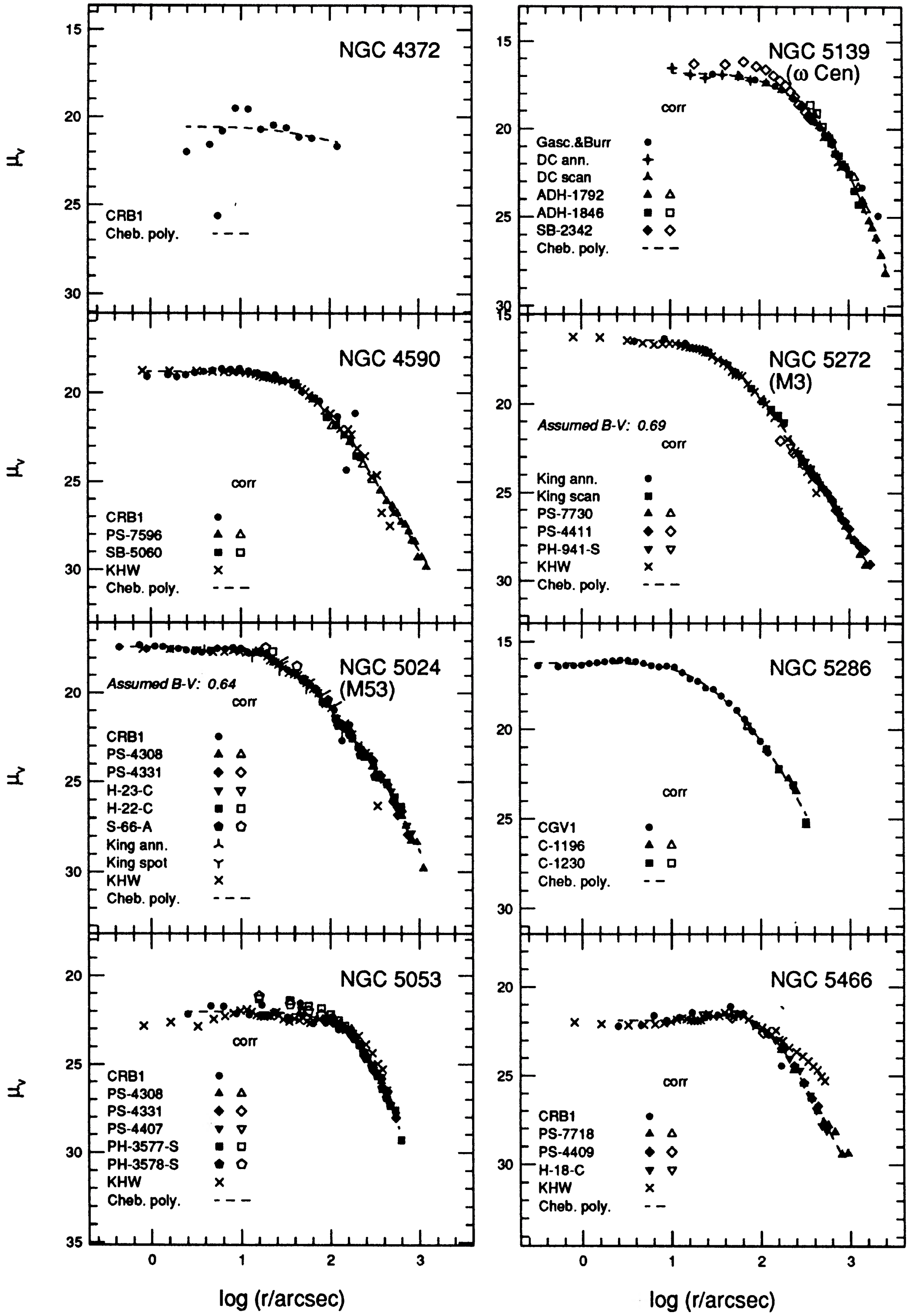

FIG. 2. (continued)

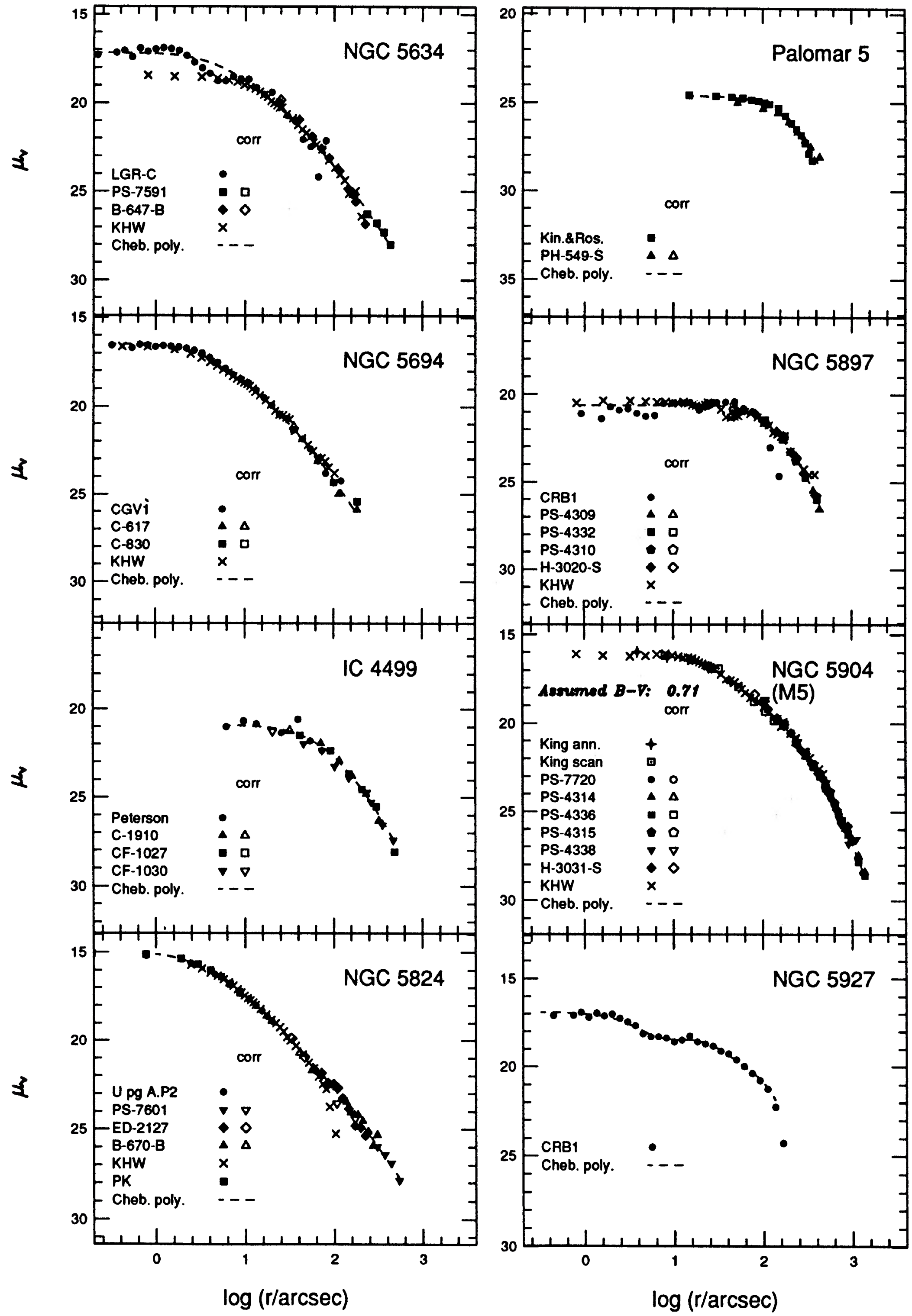

FIG. 2. (continued)

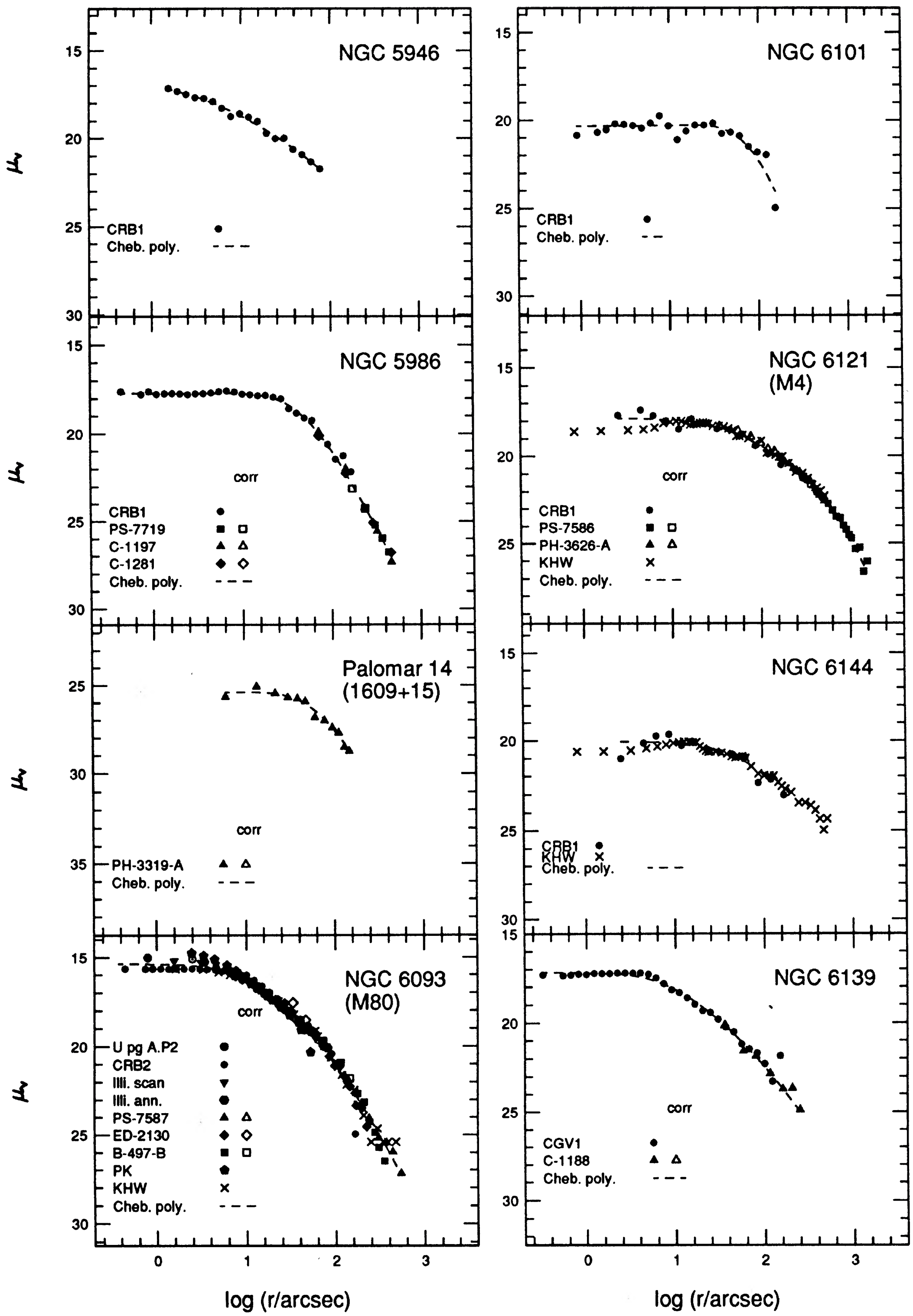

FIG. 2. (continued)

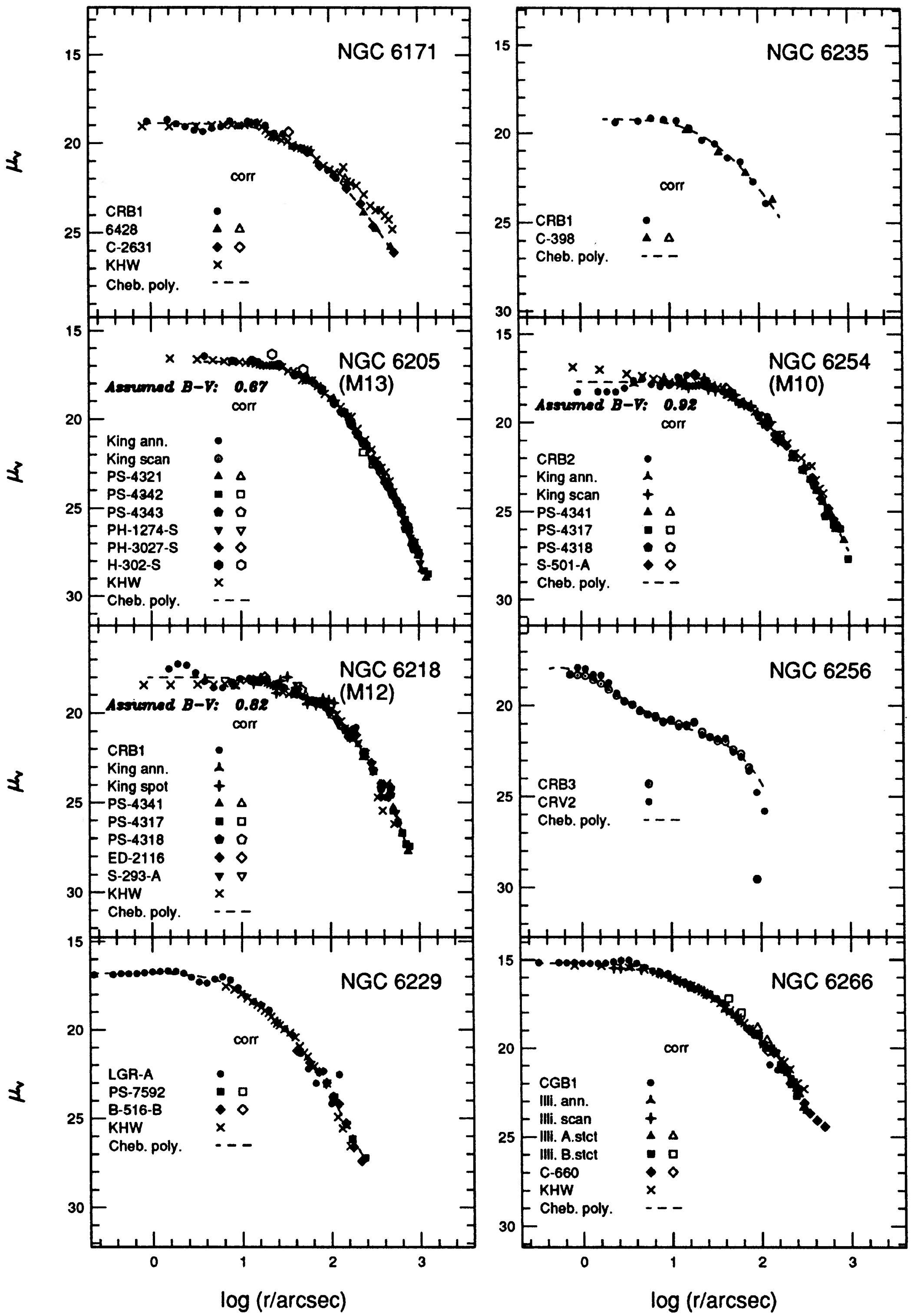

FIG. 2. (continued)

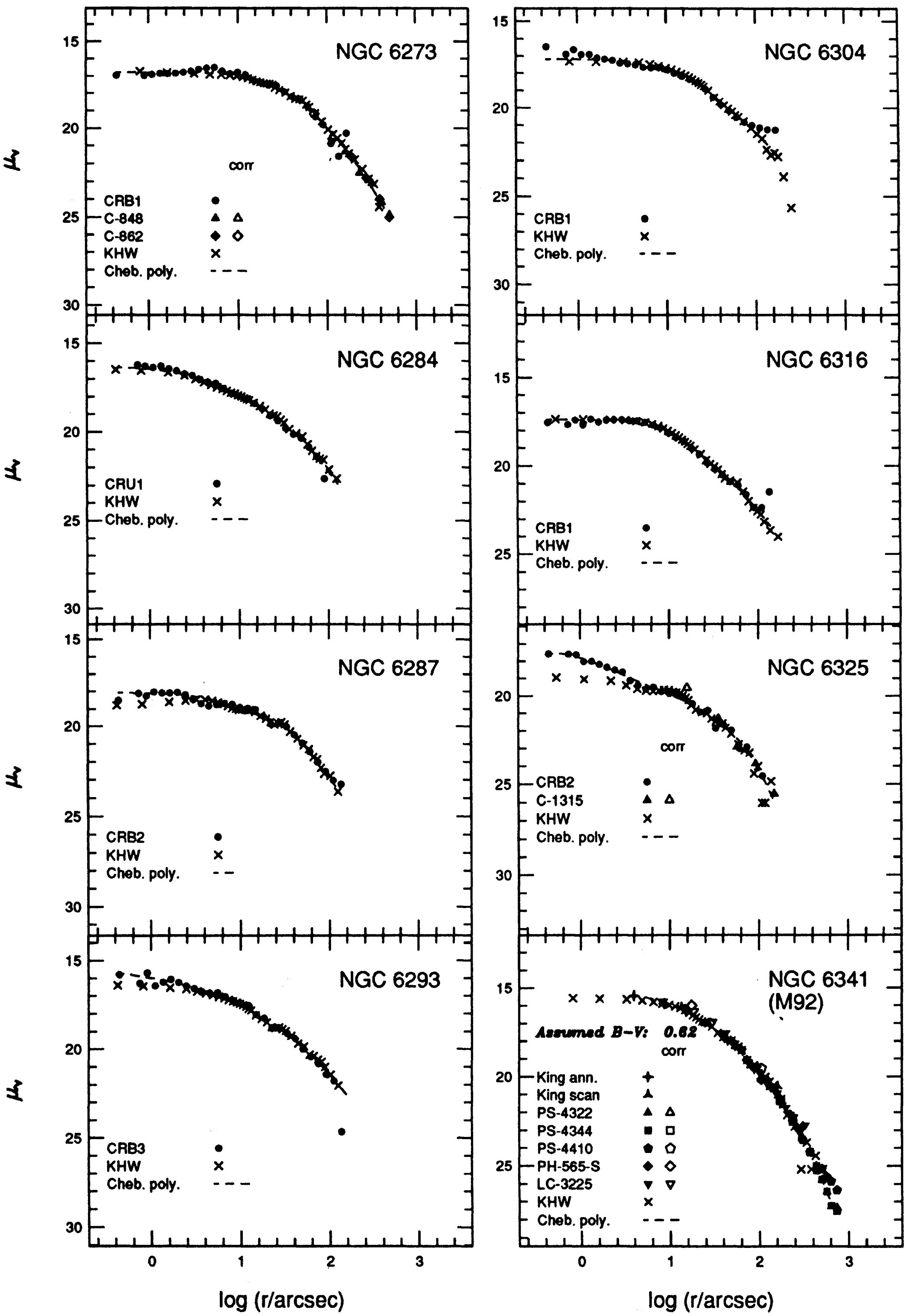

FIG. 2. (continued)

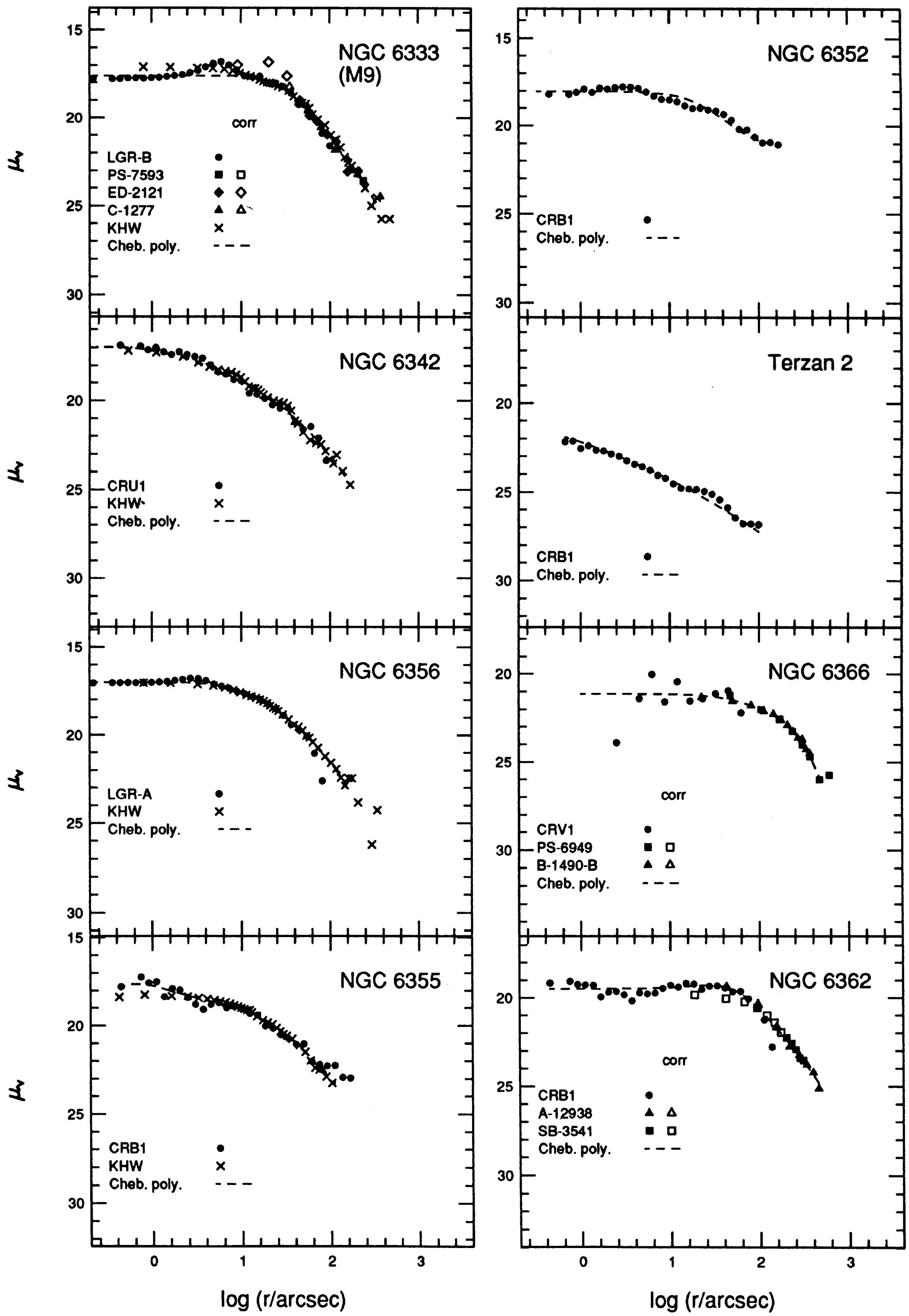

FIG. 2. (continued)

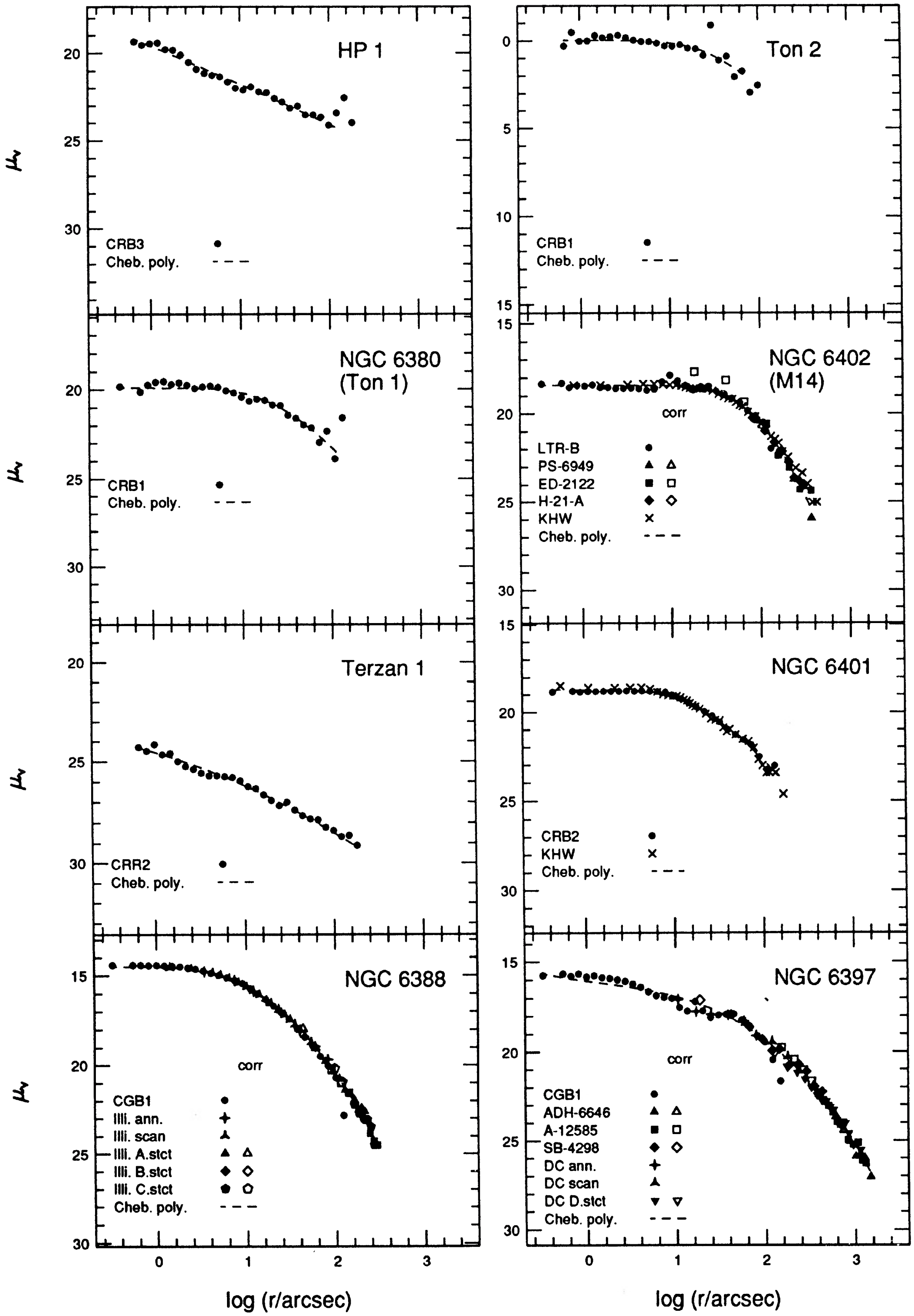

FIG. 2. (continued)

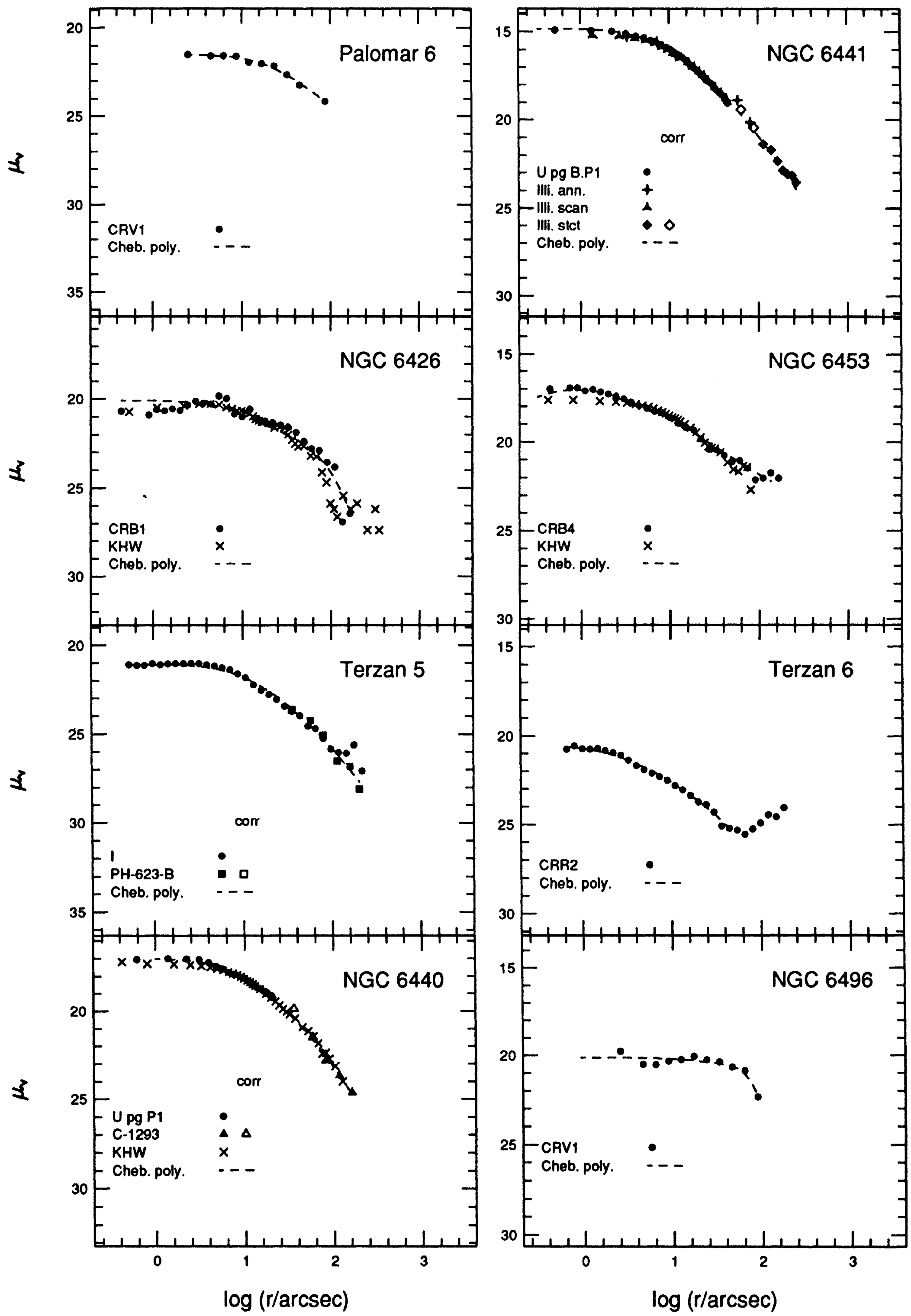

FIG. 2. (continued)

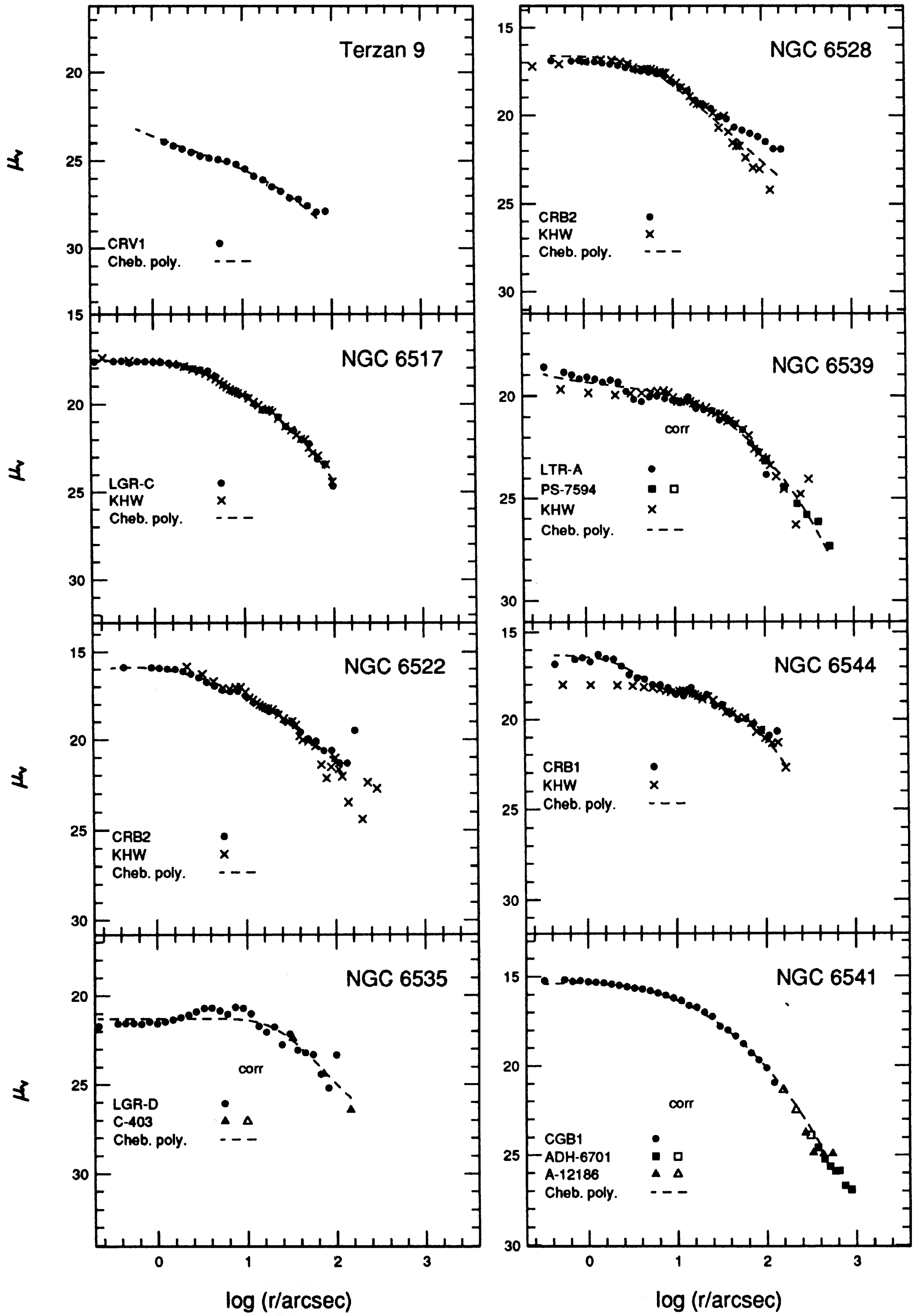

FIG. 2. (continued)

1995AJ....109..218T

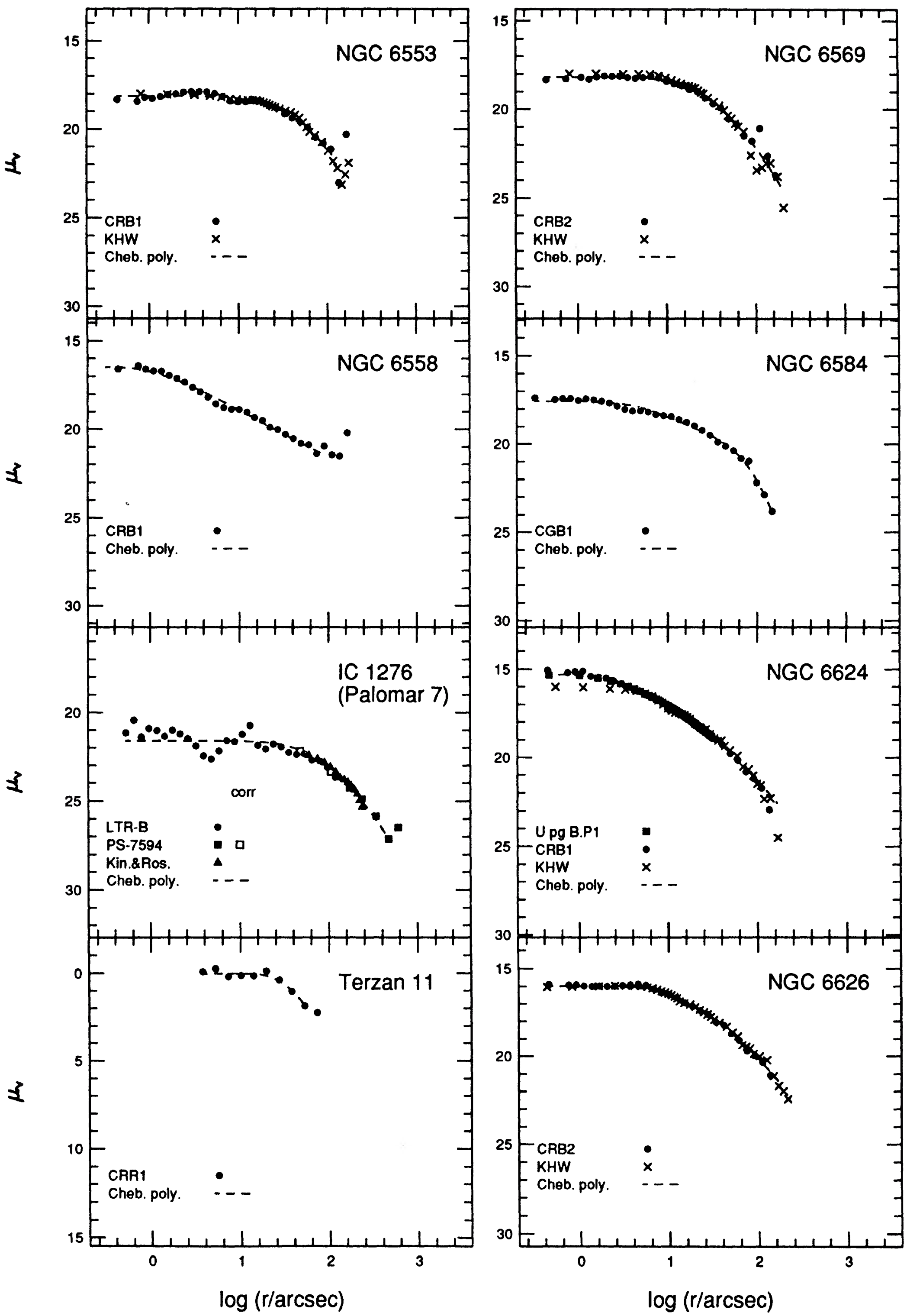

FIG. 2. (continued)

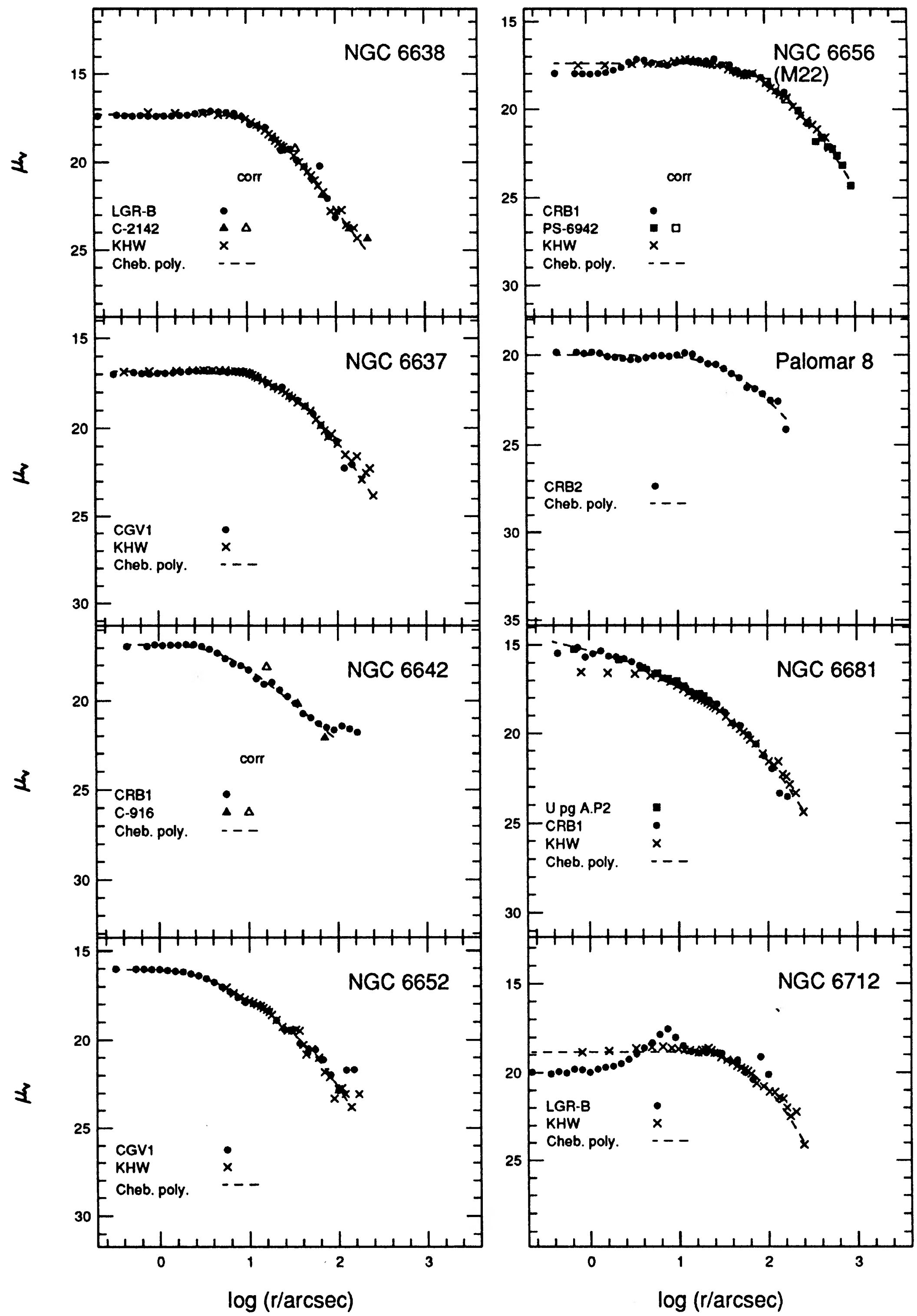

FIG. 2. (continued)

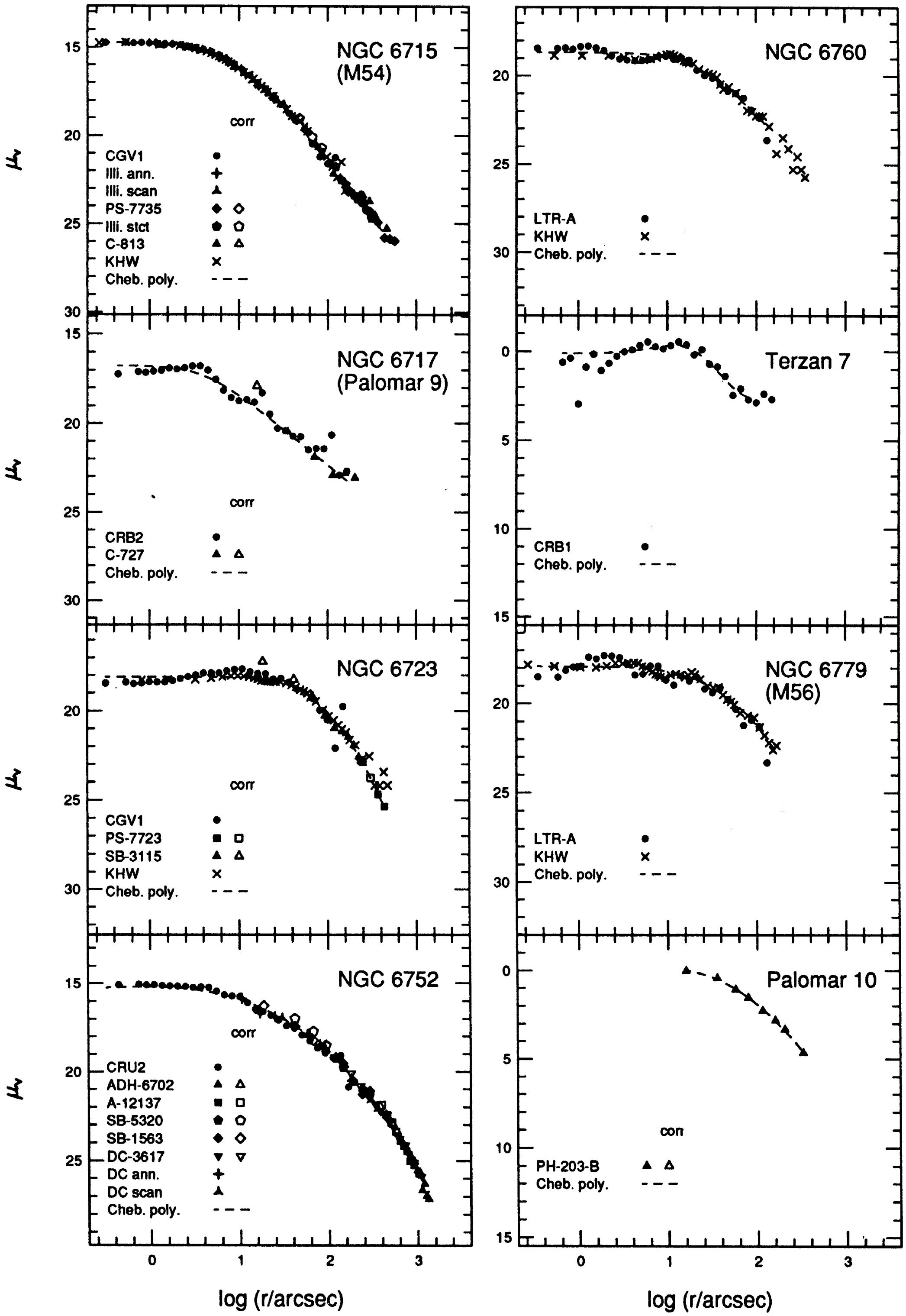

FIG. 2. (continued)

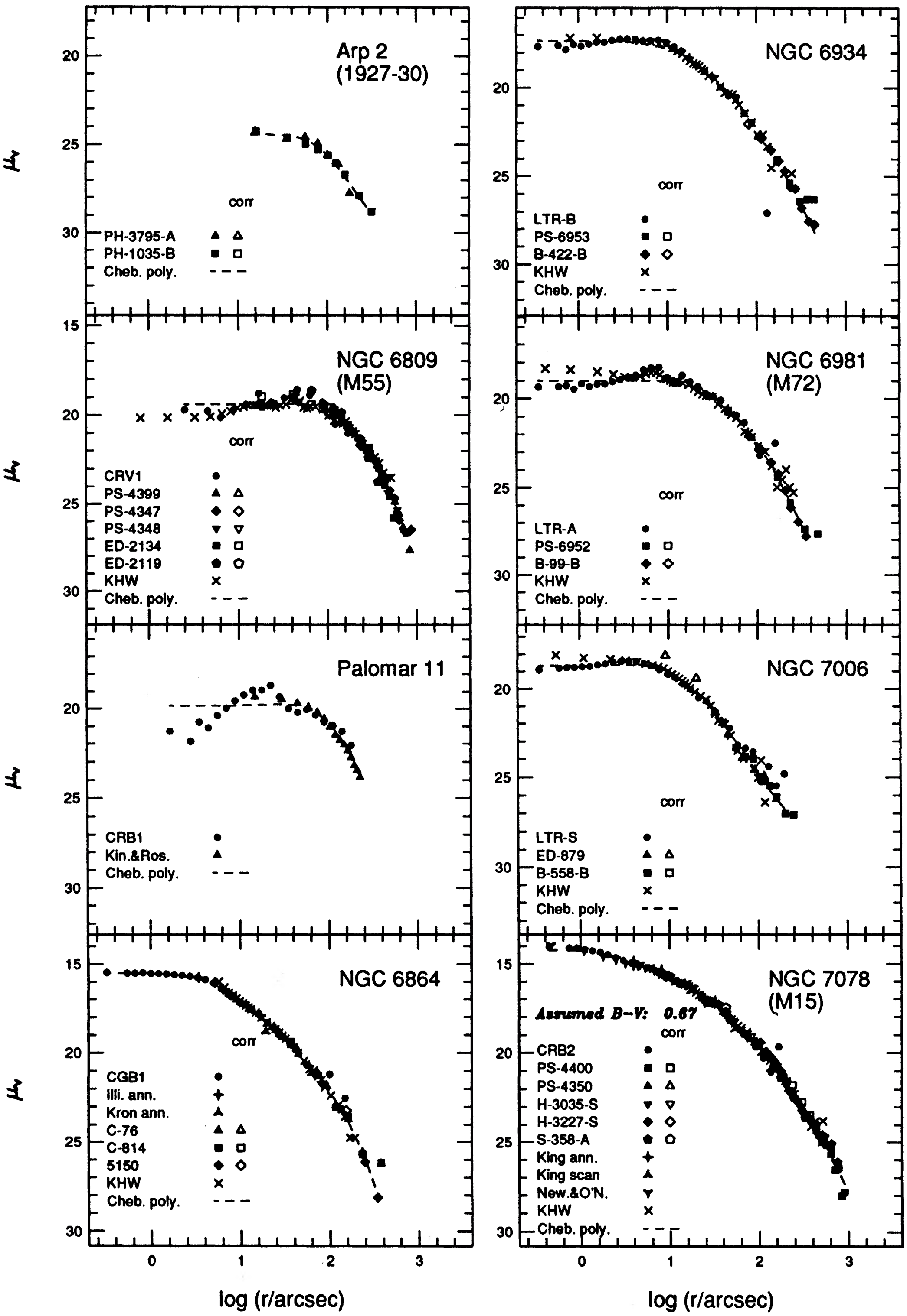

FIG. 2. (continued)

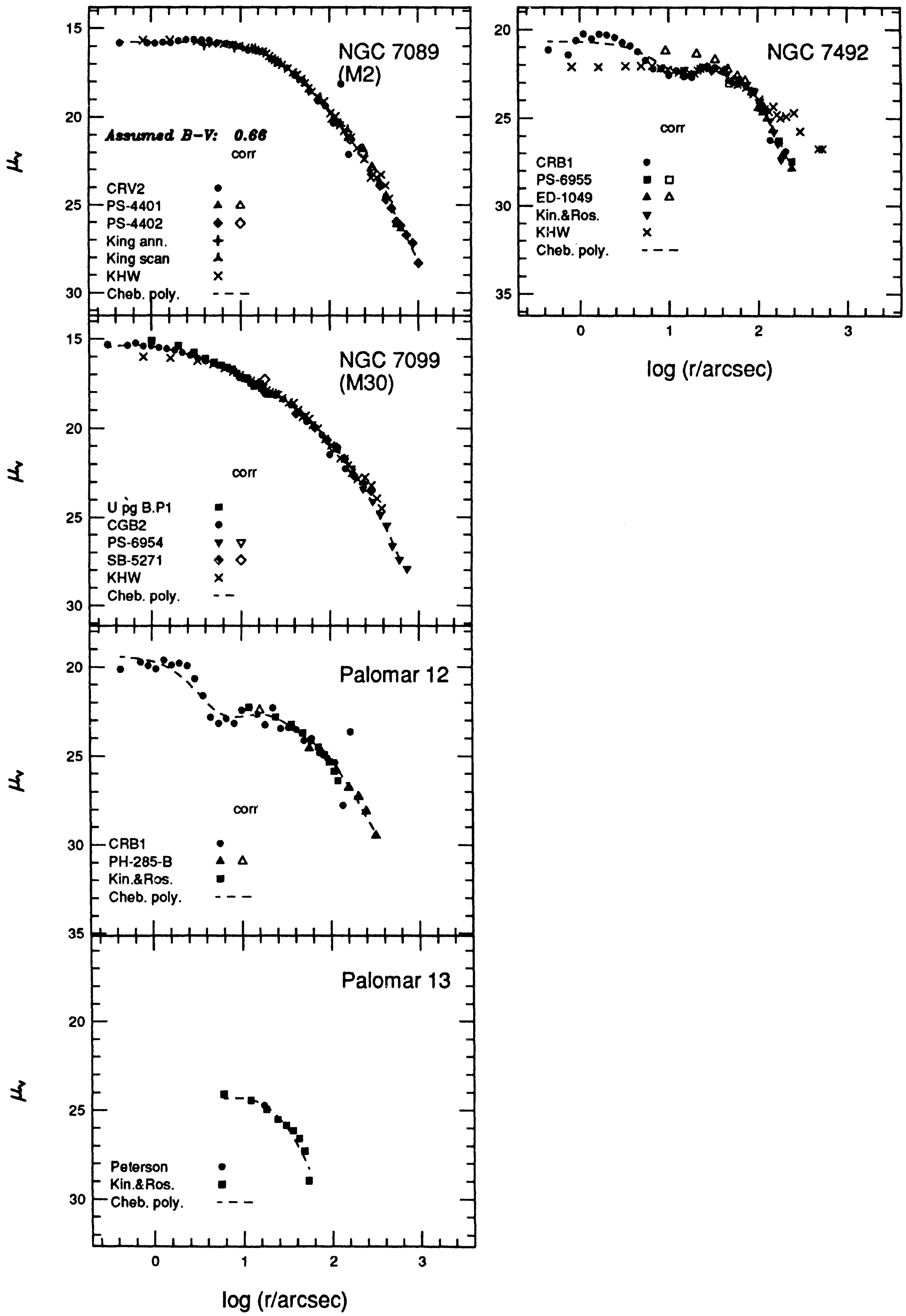

FIG. 2. (continued)

TABLE 1. Data points for SBPs. NGC 104 (47 Tuc): 6 iterations. Chebyshev coefficients $a(0)T_0(u)+a(1)T_1(u)+\cdots$, where u is log (r/arcsec) mapped to $[-1,1]$: $a(0)=19.472\pm0.112$, $a(1)=6.036\pm0.177$, $a(2)=1.130\pm0.172$, $a(3)=0.314\pm0.141$, $a(4)=0.166\pm0.138$. Power-of-x coefficients $a(0)+a(1)x+a(2)x^2+\cdots$, where $x=[1+(r/r_c)^2]$, r_c=1.42: $a(0)$=4.6828, $a(1)$=0.7515, $a(2)$=1.0310, $a(3)$=−0.3647, $a(4)$=0.0534.

log ($r/''$)	μ_V	$\mu_V^{\rm fit}$	resid.	weight	data set
−0.005	14.38	14.42	−0.04	1.0	UPGB.4
0.115	14.27	14.42	−0.15	1.0	UPGA.4
0.230	14.21	14.42	−0.21	1.0	UPGC.4
0.604	14.52	14.45	0.07	1.0	UPGB.4
0.615	14.48	14.45	0.03	1.0	UPGA.4
0.670	14.50	14.46	0.03	1.0	UPGC.4
0.707	14.57	14.47	0.10	0.8	IANN
0.723	14.57	14.47	0.10	1.0	DANN
0.802	14.61	14.50	0.12	0.8	IANN
0.822	14.62	14.51	0.11	0.8	KANN
0.881	14.54	14.53	0.01	1.0	UPGA.4
0.894	14.61	14.54	0.07	1.0	UPGB.4
0.917	14.50	14.55	−0.06	1.0	UPGC.4
0.956	14.68	14.58	0.10	1.0	ISCAN
1.002	14.70	14.62	0.09	1.0	IANN
1.050	14.62	14.66	−0.04	1.0	UPGA.4
1.072	14.76	14.68	0.08	1.0	DANN
1.074	14.73	14.69	0.04	1.0	UPGB.4
1.077	14.65	14.69	−0.04	1.0	UPGC.4
1.077	14.72	14.69	0.03	0.8	KANN
1.133	14.77	14.76	0.01	1.0	ISCAN
1.161	14.80	14.80	0.00	1.0	GBANN
1.172	14.77	14.82	−0.05	1.0	UPGA.4
1.195	14.80	14.86	−0.06	1.0	UPGC.4
1.202	14.88	14.87	0.01	1.0	UPGB.4
1.222	14.81	14.90	−0.09	1.0	IANN
1.227	14.70	14.91	−0.21	1.0	DANN
1.253	14.84	14.96	−0.12	1.0	KANN
1.258	14.94	14.97	−0.04	1.0	ISCAN
1.268	14.94	14.99	−0.05	1.0	UPGA.4
1.288	14.95	15.03	−0.08	1.0	UPGC.4
1.301	15.04	15.06	−0.03	1.0	UPGB.4
1.312	14.97	15.09	−0.12	1.0	GBANN
1.347	15.10	15.17	−0.07	1.0	UPGA.4
1.354	15.24	15.19	0.05	1.0	ISCAN
1.364	15.16	15.21	−0.06	1.0	UPGC.4
1.723	16.34	16.39	−0.05	1.0	UPGB.4
1.726	16.46	16.40	0.06	1.0	UPGC.4
1.743	16.48	16.47	0.01	1.0	UPGA.4
1.755	16.47	16.52	−0.05	1.0	UPGB.4
1.755	16.62	16.52	0.10	1.0	UPGC.4
1.762	16.44	16.55	−0.10	1.0	DANN
1.765	16.47	16.56	−0.09	1.0	KANN
1.767	16.51	16.56	−0.05	1.0	IANN
1.771	16.59	16.58	0.01	1.0	UPGA.4
1.778	16.45	16.61	−0.15	1.0	DSCAN
1.783	16.68	16.63	0.05	1.0	UPGC.4
1.785	16.54	16.64	−0.09	1.0	UPGB.4
1.798	16.71	16.69	0.03	1.0	UPGA.4
1.812	16.64	16.74	−0.11	1.0	GBANN
1.901	17.08	17.11	−0.03	1.0	DANN
1.910	17.14	17.14	0.00	1.0	IANN
1.945	17.27	17.29	−0.02	1.0	KANN
1.981	17.43	17.44	−0.01	1.0	GBANN
2.076	17.58	17.85	−0.27	0.7	SB-2074
2.079	17.89	17.86	0.02	1.0	DSCAN
2.102	17.90	17.96	−0.07	1.0	KANN
2.162	17.86	18.23	−0.37	1.0	SB-2074
2.234	18.38	18.55	−0.17	1.0	SB-2074
2.252	18.54	18.63	−0.09	1.0	KANN
2.255	18.63	18.65	−0.01	1.0	DSCAN
2.296	18.90	18.84	0.06	1.0	SB-2074
2.317	19.01	18.93	0.08	1.0	GBANN
2.350	19.18	19.09	0.09	1.0	SB-2074
2.358	19.04	19.13	−0.09	1.0	DC-3394
2.380	19.19	19.23	−0.04	1.0	DSCAN
2.398	19.44	19.32	0.12	1.0	SB-2074
2.422	19.45	19.44	0.01	1.0	KANN
2.441	19.80	19.54	0.26	1.0	SB-2074
2.444	19.54	19.55	−0.01	1.0	DC-3394
2.477	19.64	19.72	−0.08	1.0	DSCAN
2.477	19.86	19.72	0.14	0.5	GBSCAN
2.481	19.91	19.74	0.17	1.0	SB-2074
2.516	19.94	19.92	0.02	1.0	DC-3394
2.556	20.27	20.14	0.13	0.5	GBSCAN
2.578	20.08	20.26	−0.18	1.0	DC-3393
2.578	20.23	20.26	−0.03	1.0	DC-3394
2.578	20.26	20.26	0.00	0.5	DC-3416
2.623	20.63	20.51	0.11	0.3	GBSCAN
2.632	20.44	20.57	−0.13	1.0	DC-3393
2.632	20.61	20.57	0.04	1.0	DC-3394
2.632	20.61	20.57	0.04	1.0	DC-3416
2.681	20.77	20.86	−0.09	1.0	DC-3393
2.681	20.83	20.86	−0.03	1.0	DC-3416
2.681	20.88	20.86	0.02	1.0	DC-3394
2.681	20.95	20.86	0.09	0.3	GBSCAN
1.382	15.26	15.26	0.00	1.0	UPGB.4
1.388	15.23	15.28	−0.04	1.0	IANN
1.394	15.30	15.29	0.01	1.0	DANN
1.413	15.35	15.34	0.01	1.0	UPGA.4
1.424	15.34	15.38	−0.04	1.0	GBANN
1.424	15.37	15.38	−0.01	1.0	KANN
1.430	15.43	15.39	0.03	1.0	UPGC.4
1.434	15.44	15.40	0.03	1.0	ISCAN
1.450	15.50	15.45	0.05	1.0	UPGB.4
1.471	15.52	15.51	0.00	1.0	UPGA.4
1.486	15.57	15.56	0.01	1.0	UPGC.4
1.501	15.70	15.61	0.10	1.0	ISCAN
1.509	15.66	15.63	0.02	1.0	UPGB.4
1.522	15.70	15.67	0.03	1.0	UPGA.4
1.536	15.74	15.72	0.02	1.0	UPGC.4
1.559	15.82	15.80	0.02	1.0	ISCAN
1.561	15.86	15.80	0.05	1.0	UPGB.4
1.567	15.92	15.83	0.09	1.0	UPGA.4
1.581	15.98	15.87	0.11	1.0	UPGC.4
1.585	15.93	15.89	0.04	1.0	DANN
1.593	16.01	15.91	0.10	1.0	KANN
1.595	16.03	15.92	0.11	1.0	IANN
1.607	15.99	15.96	0.03	1.0	UPGB.4
1.609	16.04	15.97	0.07	1.0	UPGA.4
1.610	15.94	15.97	−0.04	0.7	ISCAN
1.621	16.09	16.01	0.07	1.0	GBANN
1.622	16.05	16.02	0.04	1.0	UPGC.4
1.647	16.12	16.11	0.02	1.0	UPGA.4
1.649	16.09	16.12	−0.03	1.0	UPGB.4
1.655	16.20	16.14	0.06	0.7	ISCAN
1.659	16.21	16.15	0.06	1.0	UPGC.4
1.661	16.31	16.16	0.15	1.0	GBANN
1.681	16.30	16.23	0.06	1.0	UPGA.4
1.688	16.22	16.26	−0.04	1.0	UPGB.4
1.694	16.31	16.28	0.03	1.0	UPGC.4
1.713	16.38	16.36	0.03	1.0	UPGA.4
2.724	21.01	21.13	−0.12	0.5	DC-3394
2.724	21.11	21.13	−0.01	0.3	DC-3407
2.724	21.11	21.13	−0.01	1.0	DC-3393
2.724	21.16	21.13	0.03	1.0	DC-3416
2.732	21.25	21.18	0.07	0.3	GBSCAN
2.763	21.37	21.38	−0.02	1.0	DC-3416
2.763	21.39	21.38	0.01	1.0	DC-3393
2.763	21.45	21.38	0.07	0.3	DC-3407
2.763	21.60	21.38	0.22	0.2	DC-3394
2.778	21.73	21.48	0.25	1.0	GBSCAN
2.800	21.54	21.64	−0.10	0.8	DC-3394
2.800	21.62	21.64	−0.02	1.0	DC-3393
2.800	21.63	21.64	−0.01	1.0	DC-3416
2.800	21.71	21.64	0.08	0.5	DC-3407
2.833	21.77	21.87	−0.09	1.0	DC-3394
2.833	21.86	21.87	−0.01	1.0	DC-3393
2.833	21.86	21.87	−0.01	1.0	DC-3416
2.833	21.96	21.87	0.09	1.0	DC-3407
2.857	21.98	22.04	−0.06	1.0	GBSCAN
2.864	22.01	22.10	−0.09	1.0	DC-3394
2.864	22.06	22.10	−0.04	1.0	DC-3416
2.864	22.13	22.10	0.03	1.0	DC-3407
2.864	22.14	22.10	0.04	1.0	DC-3393
2.890	22.24	22.30	−0.05	0.3	UP-47T
2.893	22.31	22.32	−0.01	1.0	DC-3416
2.893	22.34	22.32	0.02	1.0	DC-3393
2.893	22.34	22.32	0.02	1.0	DC-3407
2.893	22.47	22.32	0.16	1.0	DC-3394
2.920	22.48	22.53	−0.05	1.0	DC-3416
2.920	22.56	22.53	0.02	1.0	DC-3407
2.920	22.61	22.53	0.07	1.0	DC-3393
2.920	22.66	22.53	0.13	1.0	DC-3394
2.924	22.44	22.56	−0.12	1.0	GBSCAN
2.945	22.73	22.74	−0.01	1.0	DC-3407
2.945	22.79	22.74	0.05	1.0	DC-3416
2.945	22.80	22.74	0.07	1.0	DC-3393
2.945	22.83	22.74	0.09	1.0	DC-3394
2.952	22.74	22.79	−0.05	0.3	UP-47T
2.970	22.90	22.95	−0.05	1.0	DC-3407
2.970	22.94	22.95	0.00	1.0	DC-3416
2.970	23.07	22.95	0.12	1.0	DC-3393
2.982	22.90	23.05	−0.16	0.7	GBSCAN
2.992	23.04	23.14	−0.10	1.0	DC-3416
2.992	23.09	23.14	−0.04	1.0	DC-3407
2.992	23.26	23.14	0.12	1.0	DC-3393
3.005	23.02	23.25	−0.23	0.4	DC-3394
3.006	23.16	23.26	−0.10	0.8	UP-47T
3.014	23.13	23.34	−0.21	0.2	DC-3393
3.014	23.20	23.34	−0.13	1.0	DC-3407
3.014	23.23	23.34	−0.11	1.0	DC-3416
3.033	23.32	23.51	−0.20	0.5	GBSCAN
3.035	23.42	23.53	−0.11	0.6	DC-3393
3.035	23.48	23.53	−0.05	1.0	DC-3407
3.035	23.50	23.53	−0.03	1.0	DC-3416
3.054	23.75	23.71	0.04	1.0	UP-47T
3.055	23.61	23.72	−0.11	1.0	DC-3416
3.055	23.67	23.72	−0.05	1.0	DC-3407
3.055	23.78	23.72	0.06	0.5	DC-3393
3.073	23.82	23.89	−0.07	1.0	DC-3393
3.073	23.90	23.89	0.01	1.0	DC-3407
3.073	23.91	23.89	0.02	1.0	DC-3416
3.079	23.89	23.95	−0.06	0.3	GBSCAN
3.084	23.78	24.00	−0.22	0.4	DC-3394
3.092	24.04	24.08	−0.05	1.0	DC-3407
3.092	24.07	24.08	−0.01	1.0	DC-3393
3.092	24.11	24.08	0.02	1.0	DC-3416
3.097	24.15	24.13	0.02	1.0	UP-47T
3.109	24.24	24.26	−0.02	1.0	DC-3407
3.109	24.35	24.26	0.10	1.0	DC-3416
3.118	24.21	24.35	−0.14	0.5	DC-3393
3.120	24.28	24.37	−0.09	0.3	GBSCAN
3.126	24.34	24.43	−0.10	1.0	DC-3407
3.126	24.39	24.43	−0.05	0.1	DC-3416
3.137	24.35	24.55	−0.20	1.0	UP-47T
3.142	24.43	24.61	−0.18	0.0	DC-3416
3.142	24.57	24.61	−0.04	1.0	DC-3407
3.165	25.07	24.86	0.21	0.3	DC-3407
3.173	24.89	24.95	−0.06	1.0	UP-47T
3.206	25.20	25.33	−0.13	1.0	UP-47T
3.237	25.70	25.70	−0.01	1.0	UP-47T
3.266	26.18	26.07	0.11	1.0	UP-47T
3.293	27.76	26.43	1.33	0.0	UP-47T
3.319	26.97	26.78	0.19	0.5	UP-47T
3.343	27.48	27.12	0.36	0.3	UP-47T

Notes to TABLE 1

The notations in the column "dataset" are coded as follows. Photoelectric data have the initial(s) of the observer(s), followed by "ANN" for annulus or "SCAN" for local spot. U photographic surface photometry is "UPG" followed by a serial number. Entries that contain a hyphen are star counts, on the plate indicated. For further details, see the caption of Fig. 2.

error is ~0.07 in log r_h. In the cases where our data are very discrepant, the values of van den Bergh *et al.* were used.

The derived structural parameters are presented in Table 2. The clusters are listed in α_{1950} order from Djorgovski & Meylan (1993), and clusters with apparent post-core-collapse morphology are noted with a "*c*." Where a dubious measurement of r_c, c, or r_h necessitated substitution from Chernoff & Djorgovski (1989) or from van den Bergh *et al.* (1991), or where the fraction-of-light radii are particularly unreliable, a note is made. The reader can estimate the quality of the other parameters by comparing the tabulated results with the SBPs directly.

TABLE 2. Structural parameters of galactic globular clusters.

Cluster		log r_c	log r_{10}	log r_{20}	log r_{30}	log r_{40}	log r_h	c	$\mu_V(0)$	Notes
NGC 104 (47 Tuc)		1.35	1.44	1.70	1.91	2.08	2.24	2.04	14.42	
NGC 288		1.93	1.64	1.83	1.95	2.04	2.13	0.96	20.00	
NGC 362	c?	1.01	0.95	1.17	1.33	1.47	1.60	1.94	14.79	
NGC 1261		1.37	1.09	1.27	1.40	1.50	1.60	1.27	17.72	
Pal 1		1.28	0.86	1.03	1.19	1.36	1.52	1.50	22.16	1
AM 1		0.87	0.91	1.13	1.27	1.38	1.48	1.23	23.86	2
Pal 2		0.96	0.67	0.83	0.97	1.10	1.23	1.91	19.41	3, 4
NGC 1851		0.67	0.71	0.95	1.14	1.30	1.45	2.24	14.17	
NGC 1904 (M79)	c?	0.98	0.93	1.16	1.32	1.46	1.58	1.72	16.18	
NGC 2298		1.31	1.12	1.32	1.46	1.57	1.68	1.28	18.98	
NGC 2419		1.32	1.11	1.31	1.44	1.56	1.66	1.40	19.77	
NGC 2808		1.20	1.06	1.26	1.40	1.52	1.64	1.77	15.17	
Pal 3		1.46	1.11	1.29	1.41	1.51	1.60	1.00	23.06	2, 3
NGC 3201		1.94	1.64	1.82	1.95	2.06	2.16	1.31	18.96	
Pal 4		1.52	1.07	1.24	1.35	1.44	1.51	0.78	23.54	
NGC 4147		0.78	0.73	0.97	1.14	1.29	1.43	1.80	17.39	
NGC 4372		2.02	—	—	—	—	2.37	1.30	20.58	4, 5
NGC 4590		1.62	1.38	1.56	1.69	1.81	1.91	1.64	18.83	
NGC 5024 (M53)		1.35	1.24	1.45	1.60	1.73	1.85	1.78	17.37	
NGC 5053		2.13	1.75	1.92	2.03	2.12	2.20	0.82	22.03	
NGC 5139 (ω Cen)		2.19	1.95	2.14	2.26	2.37	2.46	1.24	16.81	
NGC 5272 (M3)		1.48	1.28	1.47	1.60	1.72	1.83	1.85	16.39	
NGC 5286		1.24	1.08	1.28	1.42	1.54	1.66	1.46	16.21	
NGC 5466		2.07	1.68	1.83	1.93	2.01	2.09	1.43	21.60	2, 3
NGC 5634		1.10	0.80	1.05	1.23	1.39	1.54	1.60	17.18	1
NGC 5694		0.57	0.59	0.83	1.00	1.15	1.29	1.84	16.48	
IC 4499		1.76	1.51	1.70	1.83	1.93	2.03	1.11	20.92	
NGC 5824		0.52	0.59	0.85	1.06	1.24	1.41	2.45	15.12	
Pal 5		2.24	1.80	1.97	2.08	2.17	2.25	0.74	24.67	2, 6
NGC 5897		2.07	1.63	1.80	1.91	2.00	2.09	0.79	20.60	
NGC 5904 (M5)		1.38	1.36	1.60	1.76	1.90	2.02	1.87	16.05	
NGC 5927		1.40	1.28	1.47	1.61	1.72	1.82	1.60	16.91	1, 2
NGC 5946	c	0.66	1.01	1.28	1.47	1.61	1.73	2.50	17.19	2
NGC 5986		1.58	1.24	1.41	1.53	1.63	1.72	1.22	17.70	
Pal 14 (1609+15)		1.82	1.38	1.55	1.67	1.76	1.84	0.72	25.55	2, 6
NGC 6093 (M80)		0.95	0.90	1.12	1.27	1.41	1.54	1.95	15.38	
NGC 6101		1.84	—	—	—	—	2.01	0.80	20.30	1, 5
NGC 6121 (M4)		1.70	1.79	2.02	2.19	2.32	2.43	1.59	17.88	
NGC 6144		1.75	—	—	—	—	1.99	1.55	20.05	1, 5
NGC 6139		0.91	0.96	1.21	1.38	1.54	1.67	1.80	17.18	2
NGC 6171		1.51	1.41	1.62	1.77	1.90	2.02	1.51	18.89	
NGC 6205 (M13)		1.72	1.46	1.64	1.77	1.88	1.97	1.49	16.77	
NGC 6218 (M12)		1.60	1.48	1.69	1.83	1.94	2.04	1.38	18.00	
NGC 6229		0.90	0.74	0.94	1.09	1.21	1.32	1.61	16.78	
NGC 6235		1.33	1.16	1.36	1.50	1.62	1.73	1.33	19.20	2
NGC 6254 (M10)		1.71	1.51	1.70	1.84	1.95	2.05	1.40	17.70	
NGC 6256	c	0.15	1.10	1.36	1.51	1.61	1.71	2.50	17.89	2
NGC 6266	c?	1.03	1.09	1.33	1.50	1.64	1.76	1.70	15.19	
NGC 6273		1.41	1.29	1.50	1.64	1.77	1.89	1.53	16.80	
NGC 6284	c	0.64	0.91	1.16	1.33	1.47	1.60	2.50	16.35	
NGC 6287		1.20	—	—	—	—	1.66	1.60	18.08	1, 5
NGC 6293	c	0.43	1.01	1.27	1.45	1.59	1.73	2.50	15.72	2
NGC 6304		1.10	—	—	—	—	1.93	1.80	17.20	5
NGC 6316		1.00	0.97	1.20	1.38	1.50	1.63	1.55	17.39	2
NGC 6325	c	0.26	0.93	1.19	1.35	1.48	1.58	2.50	17.56	
NGC 6341 (M92)		1.15	1.10	1.33	1.49	1.63	1.75	1.81	15.46	
NGC 6333 (M9)		1.54	1.23	1.40	1.53	1.63	1.73	1.15	17.59	
NGC 6342	c	0.45	0.92	1.18	1.37	1.51	1.64	2.50	16.97	2
NGC 6356		1.14	1.05	1.26	1.42	1.55	1.67	1.54	17.00	
NGC 6355	c	0.46	1.06	1.29	1.45	1.59	1.72	2.50	17.64	2
NGC 6352		1.70	—	—	—	—	2.09	1.10	18.03	1, 5
Terzan 2	c	0.28	1.21	1.51	1.70	1.85	1.96	2.50	22.16	2, 6
NGC 6366		2.04	1.77	1.96	2.08	2.17	2.25	0.92	21.13	
NGC 6362		1.90	1.56	1.73	1.85	1.95	2.06	1.10	19.28	2, 6
HP 1	c	0.20	1.61	1.88	2.05	2.17	2.27	2.50	21.29	2, 6, 7
NGC 6380 (Ton1)	c?	1.31	—	—	—	—	1.65	1.55	19.89	5
Terzan 1	c	0.32	1.61	1.91	2.10	2.24	2.36	2.50	25.09	2, 6
NGC 6388		0.87	0.86	1.08	1.24	1.37	1.50	1.70	14.50	
Ton 2		1.51	—	—	—	—	—	1.30	—	1
NGC 6402 (M14)		1.70	1.41	1.59	1.71	1.80	1.89	1.60	18.41	1
NGC 6401		1.17	—	—	—	—	2.06	1.69	18.70	5
NGC 6397	c	0.48	1.53	1.79	1.96	2.11	2.24	2.50	15.65	
Pal 6		1.60	—	—	—	—	—	1.10	21.51	1
NGC 6426		1.20	1.15	1.39	1.54	1.65	1.74	1.70	20.09	1
Terzan 5		1.03	1.05	1.29	1.46	1.60	1.74	1.74	21.08	2
NGC 6440		0.88	0.81	1.03	1.19	1.33	1.45	1.70	17.02	
NGC 6441		0.83	0.83	1.06	1.23	1.38	1.51	1.85	14.83	
NGC 6453	c	0.61	—	—	—	—	1.35	2.50	17.07	5
Terzan 6	c	0.52	0.72	0.98	1.16	1.30	1.42	2.50	20.76	2, 6
NGC 6496		1.80	—	—	—	—	2.05	0.70	20.12	1, 5
Terzan 9	c	0.20	1.00	1.26	1.42	1.55	1.67	2.50	23.21	2, 6
NGC 6517		0.57	0.77	1.04	1.22	1.36	1.48	1.82	17.56	
NGC 6522	c	0.49	1.03	1.30	1.49	1.65	1.78	2.50	15.75	2
NGC 6535		1.40	—	—	—	—	1.67	1.30	21.28	5
NGC 6528		0.71	—	—	—	—	1.41	2.29	16.62	5
NGC 6539		1.51	1.35	1.58	1.74	1.88	2.00	1.60	18.58	1
NGC 6544	c?	0.46	1.24	1.47	1.63	1.75	1.86	1.63	16.31	2
NGC 6541	c?	1.25	1.09	1.34	1.51	1.65	1.78	2.00	15.41	1
NGC 6553		1.52	—	—	—	—	1.97	1.17	18.14	5
NGC 6558	c	0.30	1.38	1.70	1.88	2.01	2.11	2.50	16.48	2
IC 1276 (Pal7)		1.81	1.60	1.80	1.93	2.05	2.15	1.29	21.60	2
Terzan 11		1.70	—	—	—	—	—	0.57	—	
NGC 6569		1.35	1.14	1.33	1.47	1.58	1.68	1.27	18.18	
NGC 6584		1.55	1.10	1.33	1.48	1.59	1.68	1.20	17.55	1
NGC 6624	c	0.59	0.91	1.18	1.38	1.54	1.69	2.50	15.32	2
NGC 6626 (M28)		1.16	—	—	—	—	1.97	1.67	15.99	5
NGC 6637 (M69)		1.31	1.14	1.34	1.48	1.60	1.71	1.39	16.83	
NGC 6638		1.20	0.94	1.13	1.26	1.37	1.48	1.40	17.31	
NGC 6642	c?	0.79	—	—	—	—	1.64	1.99	16.82	5
NGC 6652		0.63	0.76	1.03	1.20	1.35	1.47	1.80	16.03	
NGC 6656 (M22)		1.93	1.74	1.94	2.08	2.20	2.30	1.31	17.40	
Pal 8		1.53	—	—	—	—	1.54	1.53	20.00	5, 8
NGC 6681 (M70)	c	0.18	0.89	1.16	1.34	1.49	1.63	2.50	14.82	6
NGC 6712		1.75	1.40	1.58	1.70	1.79	1.89	0.90	18.83	2
NGC 6715 (M54)		0.81	0.76	0.98	1.14	1.29	1.44	1.84	14.75	
NGC 6717 (Pal9)	c?	0.70	—	—	—	—	1.61	2.07	16.77	5
NGC 6723		1.75	1.44	1.62	1.74	1.84	1.93	1.05	18.11	
NGC 6752	c	1.02	1.34	1.60	1.77	1.92	2.06	2.50	15.20	
NGC 6760		1.30	—	—	—	—	—	1.59	18.66	
Terzan 7		1.56	—	—	—	—	—	1.08	—	
NGC 6779 (M56)		1.34	1.24	1.45	1.59	1.70	1.80	1.37	17.91	2
Pal 10		1.68	—	—	—	—	—	1.56	—	9
Arp 2 (1927-30)		1.98	1.59	1.76	1.87	1.96	2.06	0.90	24.21	2, 6
NGC 6809 (M55)		2.23	1.77	1.93	2.04	2.13	2.21	0.76	19.40	
Pal 11		2.08	1.54	1.70	1.80	1.88	1.95	0.69	19.85	2
NGC 6864		0.76	0.72	0.95	1.13	1.29	1.43	1.88	15.53	
NGC 6934		1.17	1.00	1.20	1.34	1.46	1.57	1.53	17.33	
NGC 6981 (M72)		1.51	1.20	1.39	1.51	1.61	1.70	1.23	19.00	
NGC 7006		1.16	0.85	1.02	1.14	1.25	1.35	1.42	18.67	
NGC 7078 (M15)	c	0.61	1.04	1.30	1.49	1.64	1.78	2.50	14.21	
NGC 7089 (M2)		1.31	1.18	1.38	1.53	1.65	1.77	1.80	15.78	
NGC 7099 (M30)	c	0.54	1.05	1.33	1.51	1.66	1.79	2.50	15.35	
Pal 12		0.23	1.27	1.47	1.60	1.72	1.83	1.94	19.44	2, 3, 6, 10
Pal 13		1.46	0.93	1.08	1.18	1.26	1.33	0.66	24.31	2, 3, 6, 11
NGC 7492		1.70	1.42	1.58	1.67	1.74	1.81	1.00	20.68	1

5. SUMMARY AND FUTURE PROSPECTS

We present new SBPs of 125 Galactic globular clusters. Almost all of these SBPs are photometrically calibrated. A few clusters have SBPs for the first time. We also present structural parameters derived from our SBPs.

Several applications of the data presented here come to mind immediately. These profiles can be compared with kinematic studies to derive information on the dynamical state of the clusters (and even their IMFs), especially in the case of apparently post-core-collapse clusters. Grabhorn *et al.* (1992) have attempted this with some success, though only for two clusters, and with different data. Djorgovski & Meylan (1994) have used our structural parameters, in combination with distance, metallicity, and velocity measurements, for a multidimensional study of the history of the Galactic globular-cluster system.

However, these SBPs are not derived from strictly homogeneous material, from near the cluster centers to the outer envelope. A thorough survey of the Galactic globular-cluster system with a small telescope mounted with a large-format CCD of moderate scale could produce a much more homogeneous set of SBPs and thus derived parameters. Fischer *et al.* (1993) have made the first step in this direction with a detailed study of NGC 362 using a large-format CCD on the Las Campanas Observatory 1 m telescope. But a deep understanding of the history of the Galactic globular-cluster system may still require better measurements than we have presented here.

We wish to acknowledge the expert assistance of the CTIO and Lick Observatory staffs during the numerous observing runs. Much of the early data reduction in the Berkeley Globular Cluster Survey was done by H. Penner, C. Vuosalo, A. Oren, and C. Allen, and we thank them for their efforts. C. Peterson kindly provided his compilations of cluster photometry in electronic form. We also thank

J. J. González for providing algorithms to determine fraction-of-light radii, T. Armandroff and A. Fruchter for providing images of Terzan 5, and K. Cudworth, R. Peterson, S. Faber, M. Bolte, and P. Dubath for numerous helpful conversations. This work was supported in part by a Flintridge Foundation Fellowship to S.C.T., the NSF PYI Award No. AST-9157412 to S.D. and NASA Contract No. NAS5-28086 and Grant No. NAG5-1607 to I.R.K.

REFERENCES

Bahcall, N. A. 1976, ApJ, 204, L83
Bahcall, N. A., Lasker, B. M., & Wamsteker, W. 1977, ApJ, 213, L105
Chernoff, D., & Djorgovski, S. 1989, ApJ, 339, 904
DaCosta, G. S. 1979, AJ, 84, 505
DaCosta, G. S. 1982, AJ, 87, 990
Djorgovski, S. 1985, PASP, 97, 1119
Djorgovski, S. 1988, in Globular Cluster Systems in Galaxies, IAU Symposium No. 126, edited by J. Grindlay and A. G. D. Philip (Kluwer, Dordrecht), p. 527
Djorgovski, S., & King, I. R. 1984, ApJ, 277, L49
Djorgovski, S., & King, I. R. 1986, ApJ, 305, L61
Djorgovski, S., King, I. R., Vuosalo, C., Oren, A., & Penner, H. 1986, in Instrumentation and Research Programmes for Small Telescopes, IAU Symposium No. 118, edited by J. Hearnshaw and P. Cottrell (Reidel, Dordrecht), p. 281
Djorgovski, S., & Meylan, G. 1993, in Structure and Dynamics of Globular Clusters, ASP Conf. Ser., Vol. 50, edited by S. G. Djorgovski and G. Meylan (ASP, San Francisco), p. 203
Djorgovski, S., & Meylan, G. 1994, AJ (in press)
Djorgovski, S., & Penner, H. 1985, in Dynamics of Star Clusters, IAU Symposium No. 113, edited by J. Goodman and P. Hut (Reidel, Dordrecht), p. 73
Djorgovski, S., & Piotto, G. 1993, in Structure and Dynamics of Globular Clusters, ASP Conf. Ser., Vol. 50, edited by S. G. Djorgovski and G. Meylan (ASP, San Francisco), p. 203
Fischer, P., Welch, D. L., Mateo, M., & Côté, P. 1993, AJ, 106, 1508
Gascoigne, S. C. B., & Burr, E. J. 1956, MNRAS, 116, 570
Grabhorn, R. P., Cohn, H. P., Lugger, P. M., & Murphy, B. W. 1992, ApJ, 392, 86
Hanes, D. A., & Brodie, J. 1985, MNRAS, 214, 491
Illingworth, G., & Illingworth, W. 1976, ApJS, 30, 227
King, I. R. 1962, AJ, 67, 471
King, I. R. 1966a, AJ, 71, 64
King, I. R. 1966b, AJ, 71, 276
King, I. R. 1988, PASP, 100, 999
King, I. R., Hedemann, E., Hodge, S. M., & White, R. E. 1968, AJ, 73, 456
Kinman, T. D., & Rosino, L. 1962, PASP, 74, 499
Kron, G. E. 1966, PASP, 78, 143
Kron, G. E., Hewitt, A. V., & Wasserman, L. H. 1984, PASP, 96, 198
Kron, G. E., & Mayall, N. U. 1960, AJ, 65, 581
Newell, B., & O'Neil, E. J. 1978, ApJS, 37, 27
Peterson, C. J. 1976, AJ, 81, 617
Peterson, C. J. 1987, Astr. Data Center Bull., 1, 277
Peterson, C. J. 1993, in Structure and Dynamics of Globular Clusters, ASP Conf. Ser., Vol. 50, edited by S. G. Djorgovski and G. Meylan (ASP, San Francisco), p. 337
Peterson, C. J., & King, I. R. 1975, AJ, 80, 427
Press, W. H., Flannery, B. P., Teukolsky, S. A., & Vetterling, W. T. 1989, Numerical Recipes (Cambridge University Press, Cambridge)
Rousseau, J. 1964, Ann. d'Ap., 27, 681
Stetson, P. B. 1987, PASP, 99, 191
Trager, S. C., Djorgovski, S., & King, I. R. 1993, in Structure and Dynamics of Globular Clusters, ASP Conf. Ser., Vol. 50, edited by S. G. Djorgovski and G. Meylan (ASP, San Francisco), p. 347
van den Bergh, S., Morbey, C., & Pazder, J. 1991, ApJ, 375, 594